

Waves-vegetation interaction using generic seagrass mimics

Esti De Boever

Supervisors: Prof. dr. ir. Peter Troch, Dr. ir. Vicky Stratigaki

Counsellors: Minghao Wu, Ir. Panagiotis Vasarmidis

Master's dissertation submitted in order to obtain the academic degree of
Master of Science in Civil Engineering

Department of Civil Engineering
Chair: Prof. dr. ir. Peter Troch
Faculty of Engineering and Architecture
Academic year 2017-2018



Preface

The author gives permission to make this master dissertation available for consultation and to copy parts of this master dissertation for personal use. In all cases of other use, the copyright terms have to be respected, in particular with regard to the obligation to state explicitly the source when quoting results from this master dissertation. (01/06/2018)

This master's dissertation indicates the end of a five-year study at Ghent University to obtain the degree of Master of Science in Civil Engineering, in which I have had the opportunity to learn from the greatest professors. In particular, I would like to thank professor Peter Troch, the promotor of this thesis, who has also guided me on my Erasmus-exchange in Norway and on my internship in Jamaica.

Gratitude goes to my co-promotor Vicky Stratigaki and mentor Minghao Wu, for the guidance and knowledge concerning this thesis.

I thank all down at the Coastal Engineering department with credits to the technical staff for the set-up of the experiments: Herman, Tom, Sam and David. Without you, the experiments would not have commenced. A special gratitude goes out to Tom for handcrafting and installing the force transducers.

My colleague-student and eternal cheerleader Stephanie, with whom I've spend many days working on our theses: many thanks! You've made the endless working hours more bearable and provided me moral and emotional support in my life.

I am grateful for my water polo team, which has given me the distraction, strength and motivation to never give up.

My gratitude goes to my brother Joran, who has helped me with importing the .tdms-files in Matlab. Also my other siblings and my parents, for supporting me through these five years.

Thank you all for your encouragement!

Abstract and key words

A theoretical background is given about the attenuation of waves by seagrasses, starting from the pioneering works that treated the vegetation shoots like rigid cylinders, moving like a cantilever. Gradually, the movement of the vegetation is taken into account, and the most recent studies focussing on the posture and flexibility of the vegetation are reviewed.

Physical tests are conducted on a patch of mimics, representing *Posidonia oceanica* seagrass, in the small wave flume of the Department of Civil Engineering in Ghent. The effects of wave conditions (wave height and wave period) and meadow characteristics (flexural rigidity and submergence ratio) on wave attenuation are analysed by measuring the drag force on the blades, the wave height decay and the bending angle of the blades. Three mimics are constructed with different flexural rigidity, with three submergence ratios under regular waves with five different wave heights and wave periods, leading to a total of 200 tests.

The results show that the wave-attenuating ability of the meadow depends on the wave conditions to which it is subjected. Under larger wave heights and/or wave periods (within a restricted range), the drag force increases and an enhanced wave attenuation is obtained. The wave attenuation can further be assessed from the design characteristics of the meadow. The drag force decreases by either decreasing the submergence ratio of the stiffer mimic, by reducing the flexural rigidity of the leaves or by increasing the submergence ratio of the flexible mimic and in such a way enhancing the reconfiguration of the blades. The lower the drag force per frontal surface area, the lower the capacity of the meadow to attenuate waves.

Keywords: *Posidonia oceanica*, Artificial seagrass, Wave attenuation

Extended abstract

Seagrasses are a very widespread organism, occurring in shallow coastlines in all but the coldest saline waters on earth, and tolerating a wide range of conditions. They are a critical ecosystem that is often overlooked, while it has many functions. The most important function is the protection of coastlines from the erosive impact of waves and tides by dissipating energy and stabilizing sediments. The growing awareness of the potential of coastal vegetation like salt marshes and seagrasses in contributing to coastal protection has led to a growing number of studies to get a mechanistic understanding on how these ecosystems interact with hydrodynamics. The effects of submerged vegetation on unidirectional flows have been studied both in the field (Leonard and Luther, 1995; Neumeier and Ciavola, 2004; Thompson et al., 2004) and in the laboratory (Fonseca et al., 1982; Koch et al., 2006, Bouma et al., 2007). However, the understanding about how waves propagate through seagrass meadows and how they are affected by it are still in its infancy (Koch et al., 2006). The interaction between vegetation and oscillatory flows lacks quantification and has drawn attention of researchers in the past years. Furthermore, the influence of blade posture and flexibility remains quite unknown and has become the focus of many recent researches.

A large variability exists in wave damping and it's not possible to define a generalized behaviour of plant-induced dissipation. Therefore, adequate modelling of wave transformation along vegetation fields is of utter importance. Several studies focus on the development of expressions and parameterizations of the drag force, in which the empirical drag coefficient is implemented (Dalrymple et al., 1984; Asano et al., 1992; Kobayashi, 1993; Mendez and Losada, 1999; Bradley and Houser, 2009; Mullarney et al., 2010; Koftis et al., 2013; Maza et al., 2013). The first studies treated the vegetation like rigid cylinder, hence neglecting the movement of vegetation. However, the assumption of rigid vegetation greatly overestimates the attenuation capacity, and subsequently the movement of the vegetation is taken into account.

Given that the stiffness of different seagrass species will not likely be the same, the calibrated bulk drag coefficients only hold for one specific species. More recent studies aim to develop a straightforward, predictive framework to account for blade flexibility in wave energy dissipation models, applicable to different species (Luhar et al., 2011; Möller et al., 2014; Houser et al., 2015; Luhar et al., 2016; Paul et al., 2016 and Luhar et al., 2017). It was observed that flexible leaves are pushed over by the flow and begin to bend and move in response to the water. This reconfiguration results in a drag reduction. To take this drag reduction due to vegetation movement and flexibility into account, Luhar et al. (2011) suggest the use of the effective length l_e , defined as the length of a rigid upright blade that generates the same horizontal drag as the original flexible blade of total length h_s . The effective length accounts for drag reduction both due to a reduced frontal area and due to more streamlined shapes of the bent blades. Luhar et al. (2011) demonstrated that the reconfiguration of the vegetation in unidirectional flows depends on two dimensionless parameters: the Cauchy number Ca , and the buoyancy parameter B . For wave-induced oscillatory flows, the Keulegan-Carpenter number, KC , and the ratio of the blade length to the wave orbital excursion, L , also play a significant role (Luhar et al., 2017).

The wave attenuation depends on the vegetation characteristics (geometry, buoyancy, stiffness, density, degrees of freedom and spatial configuration) as well as the wave parameters (wave height, period and direction). Many researchers have studied the influence of different parameters with varying results (Fonseca and Cahalan, 1992; Bouma et al., 2005; Chen et al., 2007; Bradley et al., 2009; Augustin et al., 2009; Mullarney et al., 2010; Stratigaki et al., 2011; Anderson et al., 2011; Paul et al., 2012; Houser et al., 2015).

Experiments are conducted in the small wave flume with mimics representing *Posidonia oceanica* seagrass. This seagrass species is chosen due to its simple leaf geometry and its importance in the Mediterranean Sea. The effects of wave conditions (wave height and wave period) and meadow characteristics (flexural rigidity and submergence ratio) on wave

attenuation are analysed by measuring the drag force on the blades, the wave height decay and the bending angle of the blades. Wave height attenuation is obtained by measuring the wave height in front and behind the meadow and dividing the difference over the distance in between the two positions. The drag force is measured by force transducers. Shortening the mimics in between test series to obtain different submergence ratios decreases the frontal surface area of the mimics and hence reduces the drag on the mimics. To disentangle the influence of shortening the mimics and the influence of the submergence ratio, the drag force is expressed per frontal surface area of the mimic. A camera is set up next to the wave flume to measure the bending of the blades. The bending angle is defined as the angle between the blade and the vertical.

Three mimics with different flexural rigidity are constructed from notebook covers (polypropylene), plastic lids (polypropylene) and tie wraps (nylon). These materials are chosen based on previous studies with mimics of different species and have properties comparable to the real *Posidonia oceanica* plant. A patch of 91 mimics is constructed on a PVC plate of 35 cm wide and 70 cm long, yielding a shoot density of 371 shoots/m². The mimics are inserted in the board in a staggered way to avoid straight lines and thus preferential flow paths through the meadow, with their width perpendicular to the flow. The board is raised approximately 10 cm above the flume bottom, simulating the tendency of *P. oceanica* to grow on a layer of mat and allowing the force transducers to fit under the board. To prevent edge effects, the board is extended 2 m backwards and 2.5 m forwards with a slope in front. A parabolic beach is placed at the end of the flume to minimize wave reflection. Regular wave conditions with wave heights ranging from 0.02 to 0.10 m and wave periods varying between 0.9 and 2.0 s are applied with a constant water depth of 0.32 m. The lengths of the mimics are adjusted from 0.20 m, over 0.16 m, to 0.13 m to obtain three different submergence ratios. With the three different flexural rigidities of the different mimics, 25 wave conditions and three submergence ratios, a total of 200 tests is conducted.

The drag force per frontal surface area in function of the wave height is shown in Figure 1 for a wave period of 1.7 s. A linear relationship is observed between the drag force and the wave height: the higher the wave forcing, the larger the induced drag. The drag force increases with increasing flexural rigidity from mimic 2, over mimic 1, to mimic 3. The two more flexible mimics (1 and 2) show an increasing drag force with decreasing submergence ratio h_s/h , due to reconfiguration. The flexible leaves are pushed over by the wave-induced flow and the more streamlined shape in combination with the reduced frontal area results in a reduced drag. This behaviour is more pronounced for longer leaves, which explains the increased drag force with decreased submergence ratio. The phenomenon of reconfiguration is not observed for the stiffest mimic. The drag force increases with increasing wave period until the wave period equals 1.7 s, after which it decreases again.

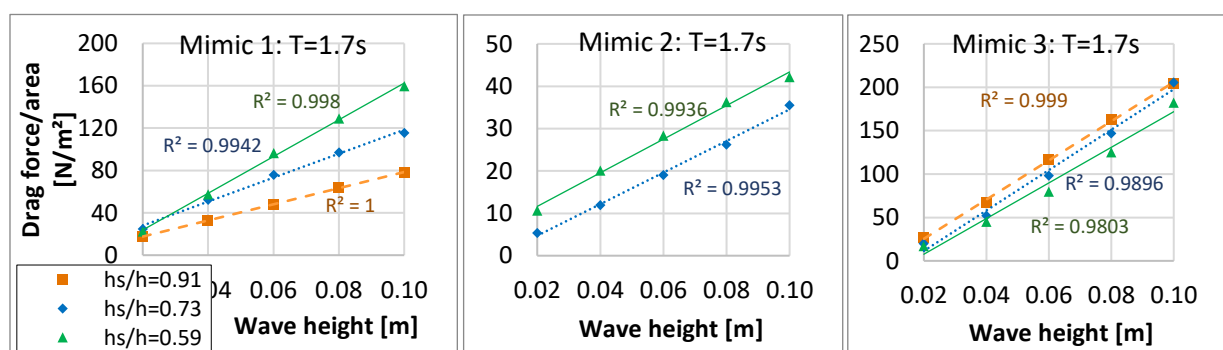


Figure 1: Drag force per frontal surface area in function of wave height

The wave height reduction in function of wave height is given in Figure 2 for a wave period of 0.9 s. A general trend is observed for which the wave height reduction increases with increasing wave height. This relationship is particularly clear for mimic 1, but does not hold for all cases. Analogously to what was found for the drag force, the wave height reduction increases with increasing submergence ratio for mimic 3 as the vegetation takes up more of the water column. No clear

conclusion about the submergence ratio can be drawn for the other mimics. For most of the cases, mimic 3 yields the largest wave height attenuation.

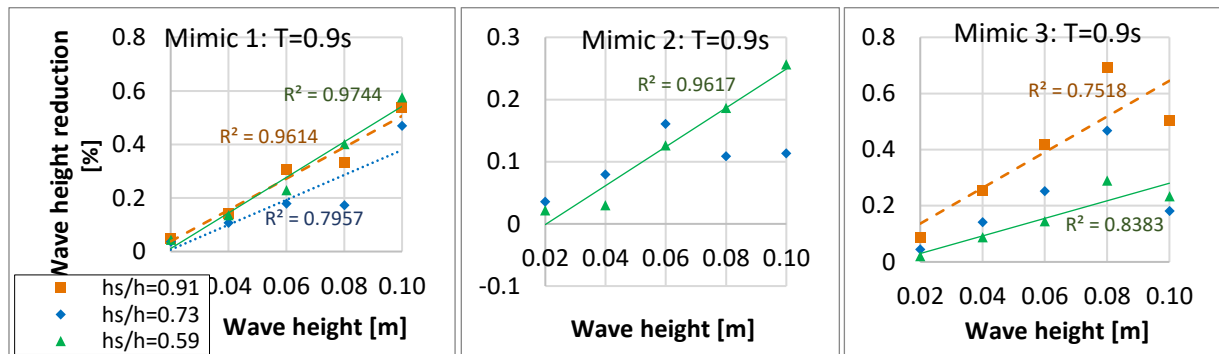


Figure 2: Wave height reduction in function of wave height

The bending angle in function of the wave height is given in Figure 3. The bending angle decreases with increasing wave height, with a very high correlation. For mimic 1 and 3, the bending angle decreases with increasing submergence ratio, while the opposite holds for mimic 2. However, for this mimic, the series with the highest submergence ratio show a residual bending in the direction of wave propagation, which results in a higher bending angle. More tests are needed to reveal whether or not this behaviour is just a coincidence. The bending angle increases with increasing flexural rigidity and with decreasing wave period.

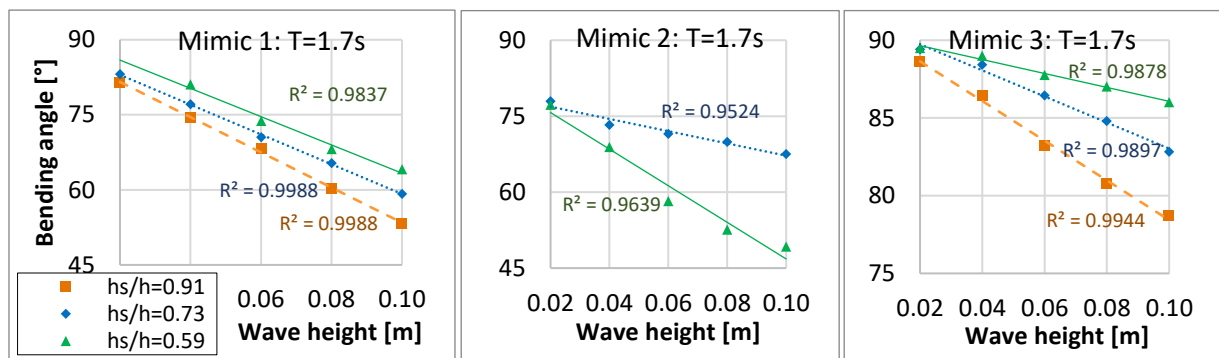


Figure 3: Bending angle in function of wave height

Combining the previous results, reveals that the drag force increases with increasing bending angle. Both the drag force and the bending angle increase with increasing flexural rigidity; as the flexibility increases, the leaves tend to avoid the drag by bending over (reconfiguration), which yields a lower bending angle and lower drag force. The reconfiguration is enhanced for higher submergence ratios, hence both the drag force and the bending angle decrease with increasing submergence ratio for the flexible mimics. This movement is not observed for the stiffer mimic 3, for which the drag force increases with increasing submergence ratio, while the bending angle decreases.

To conclude, the wave-attenuating ability of the meadow depends on the wave conditions to which it is subjected. Under larger wave heights and/or wave periods (within a restricted range), the drag force increases and hence an enhanced wave attenuation is obtained. The wave attenuation can also be assessed from the design characteristics of the meadow. From the previous, the drag force decreases by either decreasing the submergence ratio of the stiffer mimic, by reducing the flexural rigidity of the leaves or by increasing the submergence ratio of the flexible mimic and in such a way enhancing the reconfiguration of the blades. The lower the drag force per frontal surface area, the lower the capacity of the meadow the attenuate waves.

Contents

Preface.....	1
Abstract and key words.....	2
Extended abstract.....	3
Contents.....	6
List of tables.....	8
List of figures.....	8
List of abbreviations and symbols.....	9
Chapter 1: Introduction.....	11
Chapter 2: Wave attenuation by vegetation – a theoretical background.....	12
Treating the vegetation like rigid vertical cylinders, neglecting the vegetation motion.....	12
First steps to include the vegetation motion.....	16
The drag coefficient C_D	17
Determining C_D	17
Relationships between C_D and Re or KC	17
Focus on vegetation posture and flexibility.....	20
Influence of blade flexibility on C_D	25
Parameters influencing the wave attenuation by vegetation.....	26
Vegetation properties.....	26
Hydrodynamic conditions.....	28
Chapter 3: Mimics of <i>Posidonia oceanica</i>	30
The adoption of mimics.....	30
Previously used mimics.....	30
Design of the mimics.....	31
<i>Posidonia oceanica</i> properties.....	31
Mimics selection and configuration.....	33
Chapter 4: Experiment.....	36
Set-up.....	36
Test cases.....	36
Influencing parameters.....	38
Data collection.....	38
Wave gauges.....	38
Force transducers.....	39
Digital camera.....	39
Data processing.....	39
Wave gauges.....	39
Force transducers.....	40
Digital camera.....	41

Chapter 5: Sensitivity analysis.....	43
Drag force.....	43
Influence of force transducer position.....	43
Influence of wave height.....	45
Influence of submergence ratio.....	45
Influence of flexural rigidity.....	45
Influence of wave period.....	45
Wave height reduction.....	46
Influence of wave height.....	46
Influence of submergence ratio.....	46
Influence of flexural rigidity.....	46
Influence of wave period.....	46
Bending angle.....	48
Influence of wave height.....	48
Influence of submergence ratio.....	48
Influence of flexural rigidity.....	50
Influence of wave period.....	50
Combining the drag force, wave height reduction and bending angle.....	50
Conclusion.....	51
References.....	52
Appendix A.....	55

List of tables

Table 1: Relationships between drag coefficient (C_D) and Reynolds number (Re)	18
Table 2: Mimic materials used by several researchers to simulate different plant species	30
Table 3: Properties of <i>Posidonia oceanica</i>	32
Table 4: Mechanical properties of <i>Posidonia oceanica</i>	32
Table 5: Mechanical properties of the mimics compared to real <i>P. oceanica</i>	34
Table 6: Dimensionless parameters of the mimics compared to real <i>P. oceanica</i>	34
Table 7: Wave conditions	37
Table 8: Test conditions	38

List of figures

Figure 1: Drag force per frontal surface area in function of wave height	4
Figure 2: Wave height reduction in function of wave height	5
Figure 3: Bending angle in function of wave height	5
Figure 4: Global seagrass biodiversity with the number of species ranging from 1-2 (light green) to 12-15 (dark green) (Short and Green, 2003)	11
Figure 5: Schematic showing the coordinate system and force balance used to derive the mathematical model (Luhar, Nepf, 2011)	21
Figure 6: Scaling laws for wave-induced flows	24
Figure 7: Interactions of particle velocities with emergent (left) and submerged (right) stems. (Anderson et al, 2011)	27
Figure 8: Particle trajectories for shallow water (left) and deep water (right) waves. (Dean and Dalrymple, 1991)	28
Figure 9: Distribution of <i>Posidonia Oceanica</i> in the Mediterranean Sea (Vacchi et al, 2017)	32
Figure 10: <i>P. oceanica</i> plant with distinct, broad leaves and hairy remains around rhizomes (Borum et al, 2004)	33
Figure 11: Mimic design	33
Figure 12: Photographs of meadows of <i>P. oceanica</i> . (Top) illustrating the individual shoots and (Bottom) an overview of the meadow	35
Figure 13: Mimic configuration in PVC board with positions of force transducers indicated in red	36
Figure 14: Wave height reduction ΔH between WG3 and WG4 for control tests with (Z) and without stiff mimic bases (Y)	40
Figure 15: Wave height reduction ΔH between WG3 and WG5 for control tests with (Z) and without stiff mimic bases (Y)	40
Figure 16: Filter on signal of drag force for case F01	41
Figure 17: Definition of bending angle	42
Figure 18: Analysing the influence of the force transducer position	43
Figure 19: Drag force per frontal surface area at position 1 in function of wave height for different mimics and wave periods	44
Figure 20: Analysing the influence of (left) flexural rigidity on (right) wave period on the drag force	45
Figure 21: Wave height reduction in function of wave height for different wave periods and mimics	47
Figure 22: Bending angle in function of wave height for different wave periods and mimics	49
Figure 23: Analysing the influence of the flexural rigidity on the bending angle	50
Figure 24: Analysing the influence of the wave period on the bending angle	50
Figure 25: Drag force per frontal surface area in function of bending angle for different test series	51
Figure 26: Wave height reduction in function of drag force per frontal surface area for different test series	51
Figure 27: Wave height reduction in function of wave height for different wave periods and different submergence ratios	55
Figure 28: Bending angle in function of wave height for different wave periods and different submergence ratios	56

List of abbreviations and symbols

Abbreviation or symbol	Explanation
(LD)PE	(Low-density) polyethylene
a	Wave amplitude
a_0	Incident wave amplitude before entering the vegetation field (at $x=0$)
a_v	Vegetation frontal area per unit volume
A_w	Horizontal wave excursion
B	Buoyancy parameter
b_v	Blade width normal to the direction of wave propagation
c	Phase velocity
C_D	Drag coefficient
c_g	Wave group velocity
C_M	Inertia coefficient
Ca	Cauchy number
D	Damping coefficient
E	Modulus of elasticity (Young's modulus)
E_w	Wave energy density
EI	Flexural rigidity
F_B	Restoring force due to buoyancy
F_D	Drag force
F_M	Inertial force
F_S	Restoring force due to stiffness
f_w	Friction factor
F_1, F_2, F_3	Drag force measured at positions 1, 2 and 3
g	Acceleration of gravity
H	Wave height
h	Water depth
H_0	Incident wave height before entering the vegetation field (at $x=0$)
h_s	Blade height
I	Second moment of area
k	Wave number
k_s	Equivalent bottom roughness
k_v	Exponential decay coefficient (damping rate)
KC	Keulegan-Carpenter number
L	Ratio of the blade length to the wave orbital excursion
l_e	Effective length
M	Mass ratio
N	Blade density (number of blades per unit bottom area)
PA	Polyamide
PP	Polypropylene
R^2	Coefficient of determination for linear regression
Re	Reynolds number
s	Distance along the blade starting from the base

S	Slenderness number
T	Wave period
t	Blade thickness
u_b	Near-bottom orbital velocity
u_c	Characteristic velocity
u_R	Relative horizontal velocity between vegetation and water
WG	Wave gauge
β	Bending angle between the blade and the horizontal
ΔH	Wave height reduction
ϵ_v	Rate of wave energy dissipation per unit bed area
ζ	Horizontal displacement
θ	Bending angle between the blade and the vertical
λ	Wave length
λ_1	Rigidity parameter
ν	Kinematic viscosity of water
ρ	density of water
ρ_s	Solid density of the vegetation
ω	Wave angular frequency

Chapter 1: Introduction

Seagrasses are a very widespread organism, occurring in shallow coastlines in all but the coldest saline waters on earth, as depicted in Figure 4, and tolerating a wide range of conditions. Seagrasses are a critical ecosystem that is often overlooked, while it has many functions. Physically they filter coastal waters and protect coastlines from the erosive impact of waves and tides by dissipating energy and stabilizing sediments. Chemically they play a key role in nutrient cycles for fisheries and biologically they provide habitat for fish and shellfish as well as nursery areas and food to the larger ocean organisms like the manatees, dugongs and green sea turtles.

The combined effects of both anthropogenic and natural disturbances is leading to a global decline of seagrass meadows, with rates of loss estimated at 2 to 5% per year (Vacchi et al., 2017). The most important threat is the runoff of nutrients and sediments due to human activities on land. This leads to a decreased water clarity which further reduces the light penetration necessary for the seagrass to survive. Other harm is caused by shipping activities, fisheries, land reclamation and other constructions in the coastal zone (Green and Short, 2003). A major hazard is the global climate change with both physical and chemical effects, including sea level rise, augmentation of the water temperature, alteration of the wave conditions and ocean acidification. All these effects are expected to influence *P. oceanica* meadows but predictions are complex (Vacchi et al., 2017).

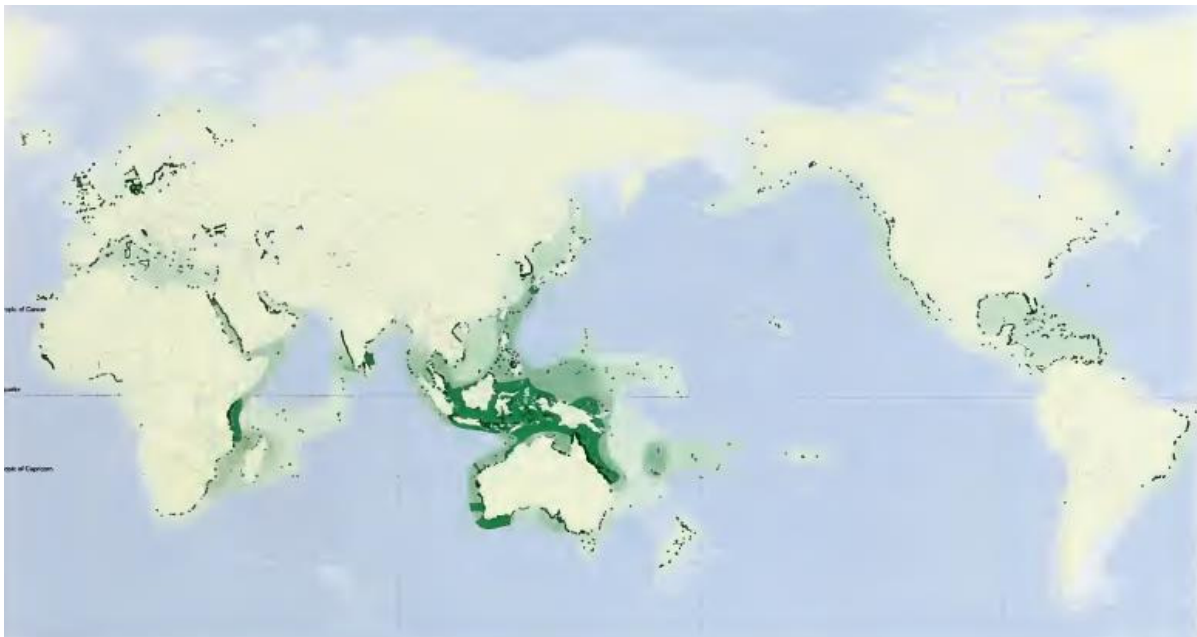


Figure 4: Global seagrass biodiversity with the number of species ranging from 1-2 (light green) to 12-15 (dark green) (Short and Green, 2003)

The growing awareness of the potential of coastal vegetation like salt marshes and seagrasses in contributing to coastal protection has led to a growing number of studies to get a mechanistic understanding on how these ecosystems interact with hydrodynamics. Extensive work has been carried out on how currents move through seagrass meadows and on how currents are affected by seagrasses and vice-versa. The effects of submerged vegetation on unidirectional flows have been studied both in the field (Leonard and Luther, 1995; Neumeier and Ciavola, 2004; Thompson et al., 2004) and in the laboratory (Fonseca et al., 1982; Koch et al., 2006; Bouma et al., 2007). However, our understanding about how waves propagate through seagrass meadows and how they are affected by it are still in its infancy (Koch et al., 2006). The interaction between vegetation and oscillatory flows lacks quantification and has drawn attention of researchers in the past years.

Chapter 2: Wave attenuation by vegetation – a theoretical background

When waves propagate through a vegetation field, they lose part of their energy due to the work they perform on the vegetation. Wave attenuation by vegetation consists of 3 components: (1) skin friction due to the surface of the plants, (2) form drag on the flow due to the shape of the plants and (3) absorption of wave energy by converting it into plant movement. Skin friction depends on the size of the wetted plant area and although this changes with the bending of flexible plants, it is often considered independent of the flow conditions. The form drag generates turbulence behind the vegetation, which dissipates energy. The transformation of wave energy into plant movement results in less energy contained in the wave and reduces the wave height (Paul et al., 2012).

The wave attenuation depends on the vegetation characteristics (geometry, buoyancy, stiffness, density, degrees of freedom and spatial configuration) as well as the wave parameters (wave height, period and direction). A large variability exists in wave damping and it's not possible to define a generalized behaviour of plant-induced dissipation. Therefore, adequate modelling of wave transformation along vegetation fields is of utter importance.

An aquatic vegetation meadow is considered, composed of rectangular blades with width (normal to the flow) b_s , height h_s and thickness t . The product of the modulus of elasticity E and the second moment of area I ($=bst^3/12$) of the leaves is the flexural rigidity of the vegetation. The density of water and the solid density of the vegetation are given by ρ and ρ_s respectively. The vegetation frontal area per unit volume is given by av and equals the product of the blade density N (blades/m²) and the blade width b_v . The meadow is subjected to wave conditions with wave height H and wave period T in a water depth h . The wave length λ is given by linear wave theory, as well as the wave number k , the phase velocity c and the angular frequency ω , which will be used later in this discussion. The coordinate x follows the direction of wave propagation and equals zero at the beginning of the meadow.

The total wave-induced force on the vegetation can be obtained from the Morison equation (Morison, 1950):

$$F = F_D + F_M = \frac{1}{2} \rho C_D h_v b_v u_R |u_R| + \frac{1}{4} \rho C_M \pi h_v b_v^2 \frac{\partial u_R}{\partial t}$$

where F_D and F_M are the drag force and inertial force respectively with corresponding drag coefficient C_D and inertia coefficient C_M and u_R is the relative velocity between the water and the vegetation. However, the inertia force has no contribution to wave attenuation because the work done by F_M per wave period equals zero. Hence, several studies focus on the development of expressions and parameterizations of the drag force.

The pioneering works providing the basis for conceptual models (Dalrymple, 1984; Kobayashi, 1993; Ghisalberti and Nepf, 2002; Mendez and Losada, 2004) neglected the vegetation motion and are based on the drag force only acting on the vegetation with each blade considered as a rigid cantilever beam with small deflections. However, the assumption of rigid vegetation significantly overestimates its ability to attenuate waves. Subsequently, the plant motion was considered and coupled to the flow field, taking the inertial forces due to buoyancy and plant stiffness into account (Asano, 1993; Dubi and Torum, 1995; Mendez, 1999). The proposed models depend on the drag coefficient, hence, this coefficient is the subject of many researches. In more recent studies, the effect of the posture of the vegetation has gained attention, together with the flexibility and scaling of the vegetation. Different parameters influencing the wave attenuation were analysed by a number of researchers.

Treating the vegetation like rigid vertical cylinders, neglecting the vegetation motion

Fonseca and Cahalan (1992) suggest that seagrass may play an important role in reducing shoreline erosion caused by wind waves. It has the ability to reduce current and wave energy, decreasing the stress on the sediment-water interface,

creating a hydrodynamic state in which local sediment resuspension is minimized. They investigated the effect of four North American seagrass species (*Zostera marina*, *Halodule wrightii*, *Syringodium filiforme* and *Thalassia testudinum*) on wave attenuation in a small wave flume, for various submergence ratios and shoot densities. They found an average of 44% reduction of wave energy per meter test section when vegetation height was almost equal to water depth.

Dalrymple et al. (1984) developed a model to calculate the combined refraction and diffraction of monochromatic linear waves and included a term to allow for wave energy dissipation. The model is based on the conservation of wave energy and is applied to rectangular regions with a spatial distribution of rigid vertical cylinders. It is assumed that linear wave theory is valid and only energy dissipation in the seagrass meadow is responsible for wave decay. The inertial forces due to the relative acceleration of water and vegetation are ignored, thus neglecting the motion of the vegetation, and the horizontal drag force is dominant. A key assumption is that the local flow field inside a canopy is not modified by the presence of the canopy elements. The bulk drag coefficient C_D accounts for all the approximations and factors not included in the formula and is constant over the water depth.

With x the direction of wave propagation, E_w the wave energy density, a the wave amplitude, c_g the wave group velocity and ϵ_v the rate of wave energy dissipation per unit bed area, the steady state energy balance is given by

$$\epsilon_v = -\frac{\partial}{\partial x}(E_w c_g) = -\frac{\partial}{\partial x}\left(\frac{1}{2}\rho g a^2 c_g\right).$$

Assuming that the dissipation is only due to drag force, neglecting both the inertia force due to the accelerating fluid and the vertical forces, and applying a standard quadratic law results in

$$\epsilon_v = F_D u = \frac{1}{T} \int_0^T \int_0^{h_s} \frac{1}{2} \rho C_D a_v u_R |u_R| u dz dt$$

in which u is the absolute horizontal velocity of the water due to the wave motion and the vertical coordinate z equals zero at the bed. By considering a different value of the bulk drag coefficient, the previous equations are taken to be valid not only for rigid plants, but also for flexible ones if the value of C_D accounts for the vegetation of motion.

As rigid vegetation moves with the flow, the relative velocity is equal to the absolute velocity and both previous equations yield a solution:

$$\frac{a(x)}{a_0} = \frac{1}{1 + K_D a_0 x}$$

With a_0 the incident wave amplitude before entering the vegetation field (at $x=0$) and K_D a constant, defined as

$$K_D = \frac{2ka_v}{9\pi} C_D \left[\frac{9 \sinh(kh_s) + \sinh(3kh_s)}{\sinh(kh) (\sinh(2kh) + 2kh)} \right].$$

The parameter K_D is made dimensionless by multiplying with the incident wave amplitude and the wave length λ :

$$K_D a_0 \lambda = \frac{4a_v a_0}{9} C_D \left[\frac{9 \sinh(kh_s) + \sinh(3kh_s)}{\sinh(kh) (\sinh(2kh) + 2kh)} \right].$$

The dimensionless parameter $K_D a_0 \lambda$ quantifies the relative decay in wave amplitude over a distance equal to the wavelength. By using the quadratic drag law, the wave decay is not exponential, as it is in most wave decay analyses.

However, for small values of the dimensionless parameter $K_0 a_0 \lambda$, the behaviour is very similar. The energy dissipation for waves propagating through a vegetation field is given by

$$\epsilon_v = \frac{2}{9\pi} \rho C_D a_v a^3 \left(\frac{kg}{\omega} \right)^3 \frac{\sinh^3(kh_s) + 3 \sinh(kh_s)}{k \cosh^3(kh)}.$$

Kobayashi et al. (1993) presented an analytical solution for monochromatic waves by using the conservation of momentum and the linear wave theory. The effect of the vegetation, regarded as rigid vertical cylinders ($u_R = u$), is taken into account by linearizing the drag force acting on the vegetation and hereby introducing an unknown damping coefficient D :

$$F_D = \frac{1}{2} \rho C_D a_v |u_R| u_R \cong \rho D u_R.$$

The local wave amplitude decays exponentially

$$\frac{a(x)}{a_0} = \exp(-k_v x)$$

with k_v , the exponential decay coefficient (or damping rate) given by

$$k_v = \frac{1}{9\pi} C_D a_v \frac{c}{c_g} \frac{g^2 k^2}{\omega^4} k H_0 \frac{\sinh^3(kh_s) + 3 \sinh(kh_s)}{\cosh^3(kh)}$$

where c and c_g are the phase velocity and group velocity respectively. The analytical solution was compared to test runs from Asano et al. (1988) and it was found that the measured wave height followed the exponential decay fairly well.

Mendez and Losada (2004) presented an empirical model for wave transformation induced by vegetation fields in variable water depths, for both monochromatic and irregular waves, including wave damping and wave breaking. The model is based on a nonlinear formulation of the drag force (Dalrymple, 1984) and considers the geometric and physical characteristics of the vegetation field, being dependent on only a single calibration parameter \tilde{C}_D , comparable to C_D . This parameter is parameterized as a function of the Keulegan-Carpenter number KC and calibrated for a specific vegetation specie (*Laminaria hyperborea*). The model is used to analyse the influence of multiple parameters on wave transformation. Forces acting on the fluid, induced by the vegetation, are expressed in a terms of a Morison-type equation neglecting swaying and inertial forces ($u_R = u$) and the horizontal force is given by the nonlinear expression of the drag force. The model is validated by the data of Lovas (2000) where *L. hyperborea* model plants were installed on a sandy 1:30 slope. For breaking conditions, the model performs very well, indicating that both breaking and vegetation contribute to the total energy dissipation.

Assuming that the fluid velocity is given by linear wave theory of the entire water depth neglects the possible reduction of wave-induced flow within the meadow. Lowe et al. (2007) showed that wave-induced velocities within meadows may be reduced significantly if the horizontal wave orbital excursion is much longer than the drag length scale of the vegetation. They developed a modelling approach to predict how flow attenuation within a submerged canopy varies among the different wave components. According to the theory, the flow will be attenuated differently among the spectral components, with greater flow occurring among the components with shorter period wave motions. Comparing the predictions with results from a field experiment confirmed that longer-period components in the spectrum are indeed significantly more attenuated compared to shorter-period components. A model for monochromatic wave dissipation predicted that rates of wave dissipation will increase as increasing flow passes through the canopy. This shows that the

rate of wave energy dissipation by a vegetation canopy is closely linked to the flow structure within the canopy, confirming what Mendez and Losada (2004) discovered earlier.

Bradley and Houser (2009) measured the blade movement and wave height decay of a natural seagrass meadow in the field under low-energy oscillatory flow. The measured wave height attenuation was found to be described well with an exponential function proposed by Kobayashi et al. (1993) and Mendez et al. (1999). They also found that seagrass is not only a wave energy attenuator but also serves as a low-pass filter. The relative motion of seagrass is not uniform at all frequencies and the seagrass should not be considered strictly as rigid or going with the flow. At the high peak frequency the seagrass moves out of phase with the current, yielding a higher relative velocity and drag, while it moves in phase for a lower secondary frequency. As wave height increases, the flow becomes more turbulent, thus reducing the ability to attenuate wave energy. At low-energy conditions the seagrass is swaying but as the oscillatory velocities increases, the seagrass bends in the direction of flow for a longer part of the wave cycle and the assumption that the stem behaves like a simple cantilever is not necessarily appropriate. For these high-energy conditions, use of a force transducer may be a more appropriate method to quantify the drag force.

Sánchez-González et al. (2011) studied wave attenuation due to seagrass meadows in a scaled (1:10) flume experiment with artificial mimics of *Posidonia oceanica*, for both regular and random waves, including the effect of wave steepness (H/λ). It was assumed that dissipation is only due to drag forces, which are linearized, neglecting the inertial forces. Furthermore, the assumption was made that the dispersion relation remained unaltered along the propagation path by vegetation presence. The equation for the energy dissipation (Dalrymple, 1984) is modified by including the wave steepness in an empirical coefficient α :

$$\epsilon'_v = \frac{1}{9\pi} \rho C_D a_v a^2 \left(\frac{kg}{\omega} \right)^3 \frac{\sinh^3(kh_s) + 3 \sinh(kh_s)}{k^2 \cosh^3(kh)} p^\alpha$$

where $p = kH_0$. By extending the meadow such that the group velocity does not vary considerably over the meadow, an exponential decay law was obtained

$$\frac{H(x)}{H_0} = \exp(-k_v x)$$

with k_v , the damping coefficient given by

$$k_v = \frac{1}{9\pi} C_D a_v \frac{c}{c_g} \frac{g^2 k^2}{\omega^4} (kH_0)^\alpha \frac{\sinh^3(kh_s) + 3 \sinh(kh_s)}{\cosh^3(kh)}$$

Hence, steeper waves were found to be mostly attenuated.

Infantes et al. (2012) used the equivalent bottom roughness k_s to calculate the friction factor f_w and the drag coefficient of a deeply submerged *Posidonia oceanica* meadow subjected to storm events mainly induced by waves. With u_b the near-bottom orbital velocity:

$$f_w = \exp \left(5.5 \left(\frac{k_s \omega}{u_b} \right)^{0.2} - 6.3 \right) = C_D a_v h_s$$

Once k_s (and subsequently f_w and C_D) are known for a certain storm, the rate of energy dissipation ϵ_v can be predicted for other storm events, following the method of Dalrymple (1984). Based on field data of a deeply submerged meadow, the value for k_s was found to be approximately 0.40 m. However, it was expected that this bottom roughness depends on the

meadow geometry, i.e. the blade length and the shoot density, so this value is not universally applicable to meadows of different geometry.

First steps to include the vegetation motion

Asano et al. (1992) extended the model of Kobayashi et al. (1993) by including the interaction between the waves and the oscillatory motion of the vegetation. In this case, the relative velocity between water and vegetation is not equal to the absolute velocity of the water ($u_R \neq u$). They analysed the flow field and the swaying motion of an individual vegetation stem hinged at the seabed. A linearized damping coefficient D links both solutions, through which the interaction effects between the waves and the vegetation motion have been accounted for. D was determined iteratively:

$$D = \frac{1}{2} C_D a_v \frac{\int_0^l u_R |u_R| u dz}{\int_0^l u^2 dz}$$

with the same definitions as used by Kobayashi et al. (1993). To take the vegetation motion into account, the length of the blades h_s was replaced by the effective height of the vegetation meadow d under wave action:

$$d = \frac{h_s + \sqrt{h_s^2 - \zeta^2}}{2}$$

with ζ the amplitude of the horizontal displacement ζ . The following calculation process was used. First the fluid velocity and complex wave number were calculated for $d=h_s$ (no vegetation motion). Subsequently the motion of vegetation was computed with:

$$\frac{1}{2} (\rho(C_M - 1) + \rho_v) V \ddot{\zeta} + \frac{1}{2} \rho C_D |u| A \dot{\zeta} + \left(\frac{8EI}{d^3} + (\rho - \rho_v) \frac{gV}{d} \right) \zeta = \frac{1}{2} \rho C_D A u |u| + \rho C_M V \dot{u}$$

with $A=b_s d$ and $V=b_s d t$. The depth-averaged value of the fluid velocity over $0 < z < d$ was taken as u . Consecutively the damping coefficient D and the height of the vegetation d were determined. The previous steps were repeated until convergence of the solution was established.

From the results, it showed that k_i increased with the drag coefficient as well as with the wave amplitude. The stiffness was increased by increasing t , but this changed the wave decay coefficient very little. The density of the vegetation also didn't have a large effect on the decay coefficient.

The results were compared with the experimental data of Asano et al. (1988) for *L. hyperborea*. Compared to the model of Kobayashi et al. (1992), the current model yielded much better agreement with the same data set, using a more realistic value of the drag coefficient of 0.5, instead of 0.1, although limits arose when the vegetation motion became large and generated turbulence.

Dubi and Tørum (1997) presented an analytical model to predict wave forces and damping for monochromatic waves, including vegetation motion. They compared three different methods to define the damping rate k_i : (1) using the analytical expression of the energy dissipation with the linearized drag force, as introduced by Dalrymple et al. (1984) and Kobayashi et al. (1993), (2) getting a numerical value of the damping rate from time series of the horizontal velocities and corresponding forces measured inside the canopy and (3) solving the complex dispersion equation for the complex wave number k by iteration. They carried out laboratory experiments to determine the damping rate k_i for *Laminaria hyperborea*, measured in terms of wave heights, forces on the vegetation and velocities inside the vegetation meadow. It was found that the damping coefficient varies with shoot density, plant size, water depth and wave period.

Mendez et al. (1999) extended the models of Kobayashi et al. (1993) and Dubi and Torum (1997) by including random waves, while taking the swaying motion of the vegetation and reflection processes into account. The buoyancy and stiffness of the vegetation are considered to be the restoring forces determining the blade motion and the dimensionless friction coefficient μ is introduced, depending on the relative motion between the fluid and the vegetation. It is assumed that the velocity of the vegetation is much smaller than that of the orbital motion.

Mullarney and Henderson (2010) derived an analytical model for the motion of single-stem vegetation subjected to waves, based on the assumption of a cantilevered beam. The model is based on the force balance between the drag force, which tends to bend the vegetation, and the elastic forces, which tend to hold the vegetation upright, and it depends mainly on the dimensionless stiffness S . The parameter S incorporates the material and geometric properties of the vegetation, as well as the wave parameters. The model is compared to in-field data of a salt marsh of *Schoenoplectus americanus*. They observed that low stiffness stems move with the surrounding water, compared to the limited motion of high stiffness stems. Low stiffness values are associated with slender stems, low Young's modulus and high-energy, high-frequency waves. Dissipation increased with increasing stiffness, depending on the frequency, as was found by Bradley and Houser (2009). High and low frequency waves are preferentially damped, while the intermediate frequencies could pass easily.

The drag coefficient C_D

The dimensionless drag coefficient C_D was introduced to account for the uncertainties and assumptions related to the vegetation-induced drag force F_D . It signifies the ability of the vegetation to reduce the hydrodynamic force (Bouma et al., 2010). Obtaining correct values for C_D is important for the prediction of wave attenuation by plants. However, the selection of appropriate C_D values for a natural vegetation meadow is challenging because it depends on a number of factors: the characteristics of the vegetated area (density, spatial configuration, location and size), the blade morphology (geometry, submergence ratio, buoyancy and rigidity), the orbital velocity and the relative water depth (Houser et al., 2015).

Determining C_D

A commonly applied method to obtain C_D is by calibrating wave dissipation models against measured wave height decay:

$$K_v = \frac{H(x)}{H_0} = \frac{1}{1 + K_D a_0 x}$$

where $K_D a_0$ is obtained by fitting the previous equation to the measured wave dissipation. C_D is derived by inverting the formula for K_D , given by Dalrymple et al. (1984).

The general calibration method to obtain C_D is prone to introducing modelling errors into the derived C_D . Furthermore, it is assumed that the wave energy loss is only due to the vegetation drag and all other dissipative processes, such as bed friction and wave breaking, are lumped into the vegetation drag, which can lead to an overestimation of C_D . Infantes et al. (2011) and Hu et al. (2014) applied a direct measuring approach to avoid these errors by measuring the total force and impact velocity on the seagrass leaves. The drag coefficient can subsequently be determined from the original Morison equation. This method can also be applied to current-wave conditions, in contrast to the calibration method which is based on models for pure wave conditions.

Relationships between C_D and Re or KC

Particularly, the drag coefficient is closely related to the Reynolds number, since it is influenced by the turbulence in meadows (Hu et al., 2014). The orbital velocity combines the role of the wave height and the water depth and is represented by the Reynolds number Re:

$$Re = \frac{u_c b_s}{\nu}$$

with ν the kinematic viscosity of water equal to 0.01 cm²/s and the characteristic fluid velocity u_c taken to be the maximum horizontal velocity at the top of the blades:

$$u_c = \omega a_0 \frac{\cosh(kh_s)}{\sinh(kh)}$$

Various different empirical relationships between the drag coefficient and the Reynolds number have been proposed for vegetation in pure wave or pure current conditions (Nepf, 2011), described by:

$$C_D = \alpha + \left(\frac{\beta}{Re}\right)^\gamma$$

where α , β and γ are the constant, coefficient and exponent of the fitted relationship. An overview is given in Table 1. The difference in relationship between C_D and Re for different researches are large and can partly be ascribed to differences in density and morphology of the vegetation, differences in relative depth and wave conditions, and/or differences in the flexibility of the vegetation. C_D decreases with increasing Re , which may be partly due to the skin friction on the surface of the vegetation affected by viscous effects. C_D decreases with increasing fluid velocity, likely due to the bending of the vegetation for higher velocities (Kobayashi et al., 1993).

Table 1: Relationships between drag coefficient (C_D) and Reynolds number (Re)

Vegetation	Study	α	β	γ
Rigid	Kobayashi et al. (1993)	0.08	2200	2.4
	Mendez et al. (1999)	0.08	2200	2.2
Semi-flexible	Maza et al. (2013)	0.87	2200	0.88
Flexible	Bradley and Houser (2009)	0.1	925	3.5
	Mendez and Losada (2004)	0.2	2	0.3
	Cavallaro et al. (2010)	0	2100	1.7
	Koftis et al. (2013)	0.77	2400	0.77
	Koftis and Prinos (2011)	0.10	2100	1.0
	Paul and Amos (2011)	0.06	240	4.0
	Maza et al. (2013)	1.61	4600	1.9

Kobayashi et al. (1993) compared their analytical solutions to test runs conducted by Asano et al. (1988) with deeply submerged, rigid mimics of *L. hyperborea*. Calibrated values for C_D were obtained for each run and varied widely in the range 0.075-1.04. The values were plotted as function of the Reynolds number Re and the following empirical relationship was found:

$$C_D = \left(\frac{2200}{Re}\right)^{2.4} + 0.08, \quad 2200 < Re < 18000$$

Applying the model of Mendez et al. (1999) to the same experimental data of Asano et al. (1988) and at first assuming no sway, gave a range of C_D from 0.09 to 1.55. These values are higher compared to the ones from Kobayashi et al. (1993), which ranged from 0.075 to 1.04. A slightly different empirical relationship between C_D and Re was obtained:

$$C_D = \left(\frac{2200}{Re}\right)^{2.2} + 0.08, \quad 200 < Re < 15500 .$$

Considering the motion of the vegetation, C_D increased and ranged from 0.33 to 6.9, because a lower velocity relative to the plant when accounting for plant motion requires a higher drag coefficient to maintain the same amount of wave energy attenuation. The empirical relationship including the swaying motion is:

$$C_D = \left(\frac{4600}{Re}\right)^{2.9} + 0.4, \quad 2300 < Re < 20000 .$$

The correlation coefficient was improved which suggests that swaying motion of the vegetation needs to be considered for optimal drag estimation.

Bradley and Houser (2009) studied a natural seagrass meadow in the field under oscillatory flow under low-energy conditions. The vegetation is assumed to be rigid, which yields an underprediction of the drag coefficients to achieve the observed wave energy decay. They identified a relationship between the drag coefficient and the Reynolds number for *Thalassia testudinum*:

$$C_D = \left(\frac{925}{Re}\right)^{3.16} + 0.1, \quad 200 < Re < 800 .$$

This relationship suggests that the vegetation is swaying at low-energy conditions but becomes increasingly rigid when the oscillatory velocities increase, extending the seagrass in the direction of flow for a larger part of the wave cycle.

Hu et al. (2014) found the following empirical relationship between the drag coefficient and the Reynolds number:

$$C_D = \left(\frac{730}{Re}\right)^{1.37} + 1.04, \quad 300 < Re < 4700 .$$

in which Re is defined using the in-canopy measured velocity U_{max} , in contrast to earlier studies where the velocity in front of the canopy U_w was taken as the characteristic velocity for determining Re . U_{max} directly interacts with the mimics, which is more representative for the hydrodynamic conditions inside a meadow. They also found that the drag coefficient in current-wave conditions is a fraction of the one in pure wave cases, i.e. $C_{D-current} = 0.66 C_{D-waves}$. The presence of a current reduces C_D since the Reynolds number is increased.

Other researchers suggested relations between the drag coefficient and the Keulegan-Carpenter number (Mendez and Losada, 2004; Sanchez-Gonzalez, 2011; Infantes et al., 2012; Jadhav et al., 2013), which is the ratio of the length scale of the wake to the length scale of the vegetation meadow:

$$KC = \frac{u_c T_p}{w}$$

with T_p the peak wave period and w either the width of the blades, the spacing in between the shoots or the distance that the blade bends in the flow.

Mendez and Losada (2004) validated their model by comparing the solution to the experimental results of Dubi et al. (1995) for the very flexible *L. hyperborea*. To fit the experimental data, an average bulk drag coefficient \tilde{C}_D was proposed which is independent of the wave height and depends on the flow around the plants and the plant motion, unlike Dalrymple et al. (1984) who assumed that the local flow field inside the canopy remains unaltered by the presence of the canopy elements. They performed a simplified analysis, avoiding the plant motion and focusing on the hydrodynamic processes.

They found a more suitable relation for correlating the drag coefficient with the incident wave parameters using the Keulegan-Carpenter number:

$$\tilde{C}_D = 0.47 \exp(-0.052KC), \quad 3 \leq KC \leq 59$$

where the plant area per unit height a_v is taken for w in the formula for KC and the characteristic velocity is the maximum horizontal velocity acting on the vegetation at the middle of the vegetation field. The best relation for \tilde{C}_D as a function of KC and the relative vegetation height h_s/h was obtained with a modified Keulegan-Carpenter number Q :

$$\tilde{C}_D = \frac{\exp(-0.0138Q)}{Q^{0.3}}, \quad 7 \leq Q \leq 172 \quad \text{and} \quad Q = \frac{K}{(h_s/h)^{0.76}}$$

This relation for near-emergent cases was confirmed by Augustin et al. (2009). They conducted laboratory experiments on mimics of *Spartina alterniflora* to measure wave attenuating on emergent and nearly emergent wetland vegetation, under a range of wave conditions and shoot densities. Both rigid mimics fabricated from cylindrical wooden dowels as well as flexible elements constructed out of polyethylene foam tubing were analysed with lengths of 30 cm.

Physical model tests were conducted on mimics made from polypropylene and polyethylene in the average wave climate of the Mediterranean Sea by Sánchez-González et al. (2011). The drag coefficient showed correlation with both the Reynolds number and the Keulegan-Carpenter number. For both parameters, the maximum orbital velocity at the top of the blades is again taken as the characteristic velocity (Kobayashi, 1993). Like Mendez and Losada (2004), they obtained that the drag coefficient C_D is better described by the Keulegan-Carpenter number KC than by the Reynolds number Re for oscillatory flow:

$$C_{D,SG} = \frac{22.9}{KC^{1.09}}, \quad 15 \leq KC \leq 425.$$

The regular wave heights predicted by this method were compared to the measure wave heights and a high correlation ($R^2=0.982$) was found. Evaluating this expression for random waves gave a correlation of $R^2=0.991$, making the model adequate for both monochromatic and random waves. Kobayashi (1993) obtained a similar expression of the damping coefficient with α equal to 1. Evaluating this value of the drag coefficient for the regular waves yielded

$$C_{D,Kob} = \frac{35.5}{KC^{1.12}}, \quad 15 \leq KC \leq 425.$$

This expression was validated for the random wave tests and it was found that this set correlated well with KC ($R^2=0.944$), despite a general trend for slight overestimation. Mendez and Losada (2004) obtained a different wave attenuation law in which $K_{D\alpha_0}$ equals the expression for the damping coefficient k_v from Kobayashi (1993). Applying this attenuation law to the measured regular wave heights yielded the drag coefficient

$$C_{D,ML} = \frac{39.5}{KC^{1.08}}, \quad 15 \leq KC \leq 425$$

which showed good correlation ($R^2=0.987$) for the random waves (Sánchez-González et al., 2011).

Focus on vegetation posture and flexibility

The previously discusses drag coefficients are mostly based on the Reynolds number or the Keulegan-Carpenter number, which can account for the changes in hydrodynamic conditions, however, they do not take the flexibility of the plant into account. Given that the stiffness of different seagrass species will not likely be the same, the calibrated bulk drag

coefficients only hold for one specific species (Luhar et al., 2016). The following studies aim to develop a straightforward, predictive framework to account for blade flexibility in wave energy dissipation models, applicable to different species.

Luhar et al. (2011) demonstrated that the reconfiguration of the vegetation in unidirectional flows depends on two dimensionless parameters: the Cauchy number Ca , and the buoyancy parameter B . They studied the effect of unidirectional steady flow on vegetation posture and drag by a combination of theoretical modelling and laboratory flume experiments. The theoretical model is based on the force balance between the hydrodynamic drag force and the restoring forces due to vegetation buoyancy and stiffness. When the drag force is small compared to the restoring forces, the blade remains upright; when the drag force exceeds the restoring forces, the blades are pushed over by the flow. Based on the characteristics of seagrasses, only individual flexible blades with uniform rectangular cross-section are considered, but the model can be extended to analyse more complicated geometries. Luhar et al. (2011) assume steady flow with form drag as the dominant hydrodynamic force and negligible viscous skin friction. Figure 5 shows the used coordinate system with s the distance along the blade starting from the base and θ the local bending angle between the blade and the vertical.

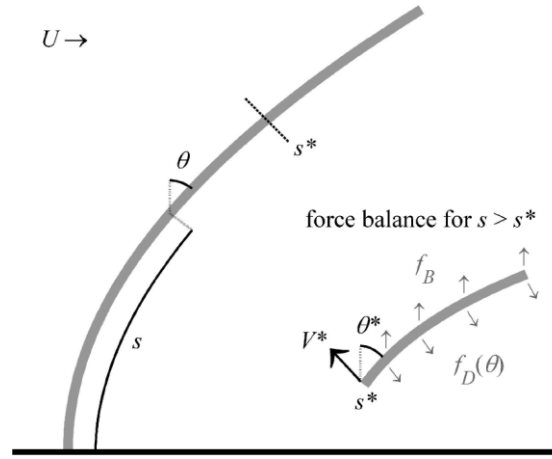


Figure 5: Schematic showing the coordinate system and force balance used to derive the mathematical model (Luhar, Nepf, 2011)

The force drag per unit length is given by

$$f_D = \frac{1}{2} \rho C_D b_s U^2 \cos^2 \theta .$$

The vertical restoring force per unit length due to buoyancy (f_B) and the restoring force due to stiffness (V), normal to the blade, are

$$f_B = (\rho - \rho_v) g b_s t \quad \text{and} \quad V = -EI \frac{d^2 \theta}{ds^2}$$

Balancing the forces, using the expressions and making the equation dimensionless by replacing s with $\hat{s} = s/h_s$ yields

$$-\frac{d^2 \theta}{d\hat{s}^2} \Big|_{\hat{s}^*} + B(1 - \hat{s}^*) \sin \theta^* = Ca \int_{\hat{s}^*}^1 \cos(\theta - \theta^*) \cos^2 \theta d\hat{s}$$

with s^* an arbitrary position along the blade and θ^* the corresponding bending angle at that position. This equation indicates that posture is controlled by two dimensionless parameters: the Cauchy number Ca and the buoyancy parameter

B. Ca indicates the relative magnitude of the hydrodynamic drag (F_D) and the restoring force due to stiffness (F_S), B represents the ratio of the restoring force due to buoyancy (F_B) and the restoring force due to stiffness (F_S).

$$Ca = \frac{F_D}{F_S} = \frac{1}{2} \frac{\rho C_D b_s U^2 h_s^3}{EI}, \quad B = \frac{F_B}{F_S} = \frac{(\rho - \rho_s) g b_s t h_s^3}{EI}$$

When the hydrodynamic forcing is much smaller than the restoring force due to stiffness $Ca \ll 1$ or due to buoyancy $Ca \ll B$, the blade remains upright in the flow. As the velocity increases such that the hydrodynamic forcing becomes larger than the restoring forces, $Ca > 0(1)$ and $Ca > 0(B)$, the blade is pushed over by the flow, it begins to bend and move in response to the water. This reconfiguration results in a drag reduction. To take this drag reduction due to vegetation movement and flexibility into account, Luhar et al. (2011) suggest the use of the effective length l_e , as introduced before (Luhar et al., 2010). This effective length is the length of a rigid upright blade that generates the same horizontal drag as the original flexible blade of total length h_s . Over this effective length, the blade moves significantly with respect to the water, while the upper part of the blade moves passively with the flow. As the ability of the vegetation to reduce wave energy depends on the relative motion between the vegetation and the fluid, the energy dissipation of flexible vegetation with total length h_s can be calculated by assuming rigid vegetation with an effective length l_e instead. The effective length accounts for drag reduction both due to a reduced frontal area and due to more streamlined shapes of the bent blades. The following empirical relationship is suggested, based on model predictions for zero-stiffness and zero-buoyancy cases:

$$\frac{l_e}{h_s} = 1 - \frac{1 - 0.9Ca^{-1/3}}{1 + Ca^{-3/2}(8 + B^{3/2})}$$

When the hydrodynamic forcing becomes much larger than the restoring forces, $Ca \gg B$ and $Ca \gg 1$, the effective length scales as $l_e/h_s \sim Ca^{-1/3}$. If blade stiffness is the dominant restoring force, the drag force F_D is proportional to the flow velocity U according to $F_D \propto U^{4/3}$. If the dominant restoring force is the blade buoyancy, the scaling becomes sub-linear, $F_D \propto U^a$, with $a < 1$. For steady flows with $B \gg 1$, the additional restoring force due to buoyancy delays the onset of reconfiguration until the Cauchy number exceeds the buoyancy parameter, $Ca \gg B$. Blade stiffness will be the dominant restoring mechanism when the hydrodynamic forcing becomes significantly larger than the blade buoyancy and the effective length will be independent of the buoyancy parameter B . Only closer to the top of the blades, the effect of buoyancy becomes more discernible, but due to the near-horizontal orientation at the top, no significant drag is generated. Therefore, blade buoyancy does not significantly affect the generated drag and the effective length becomes independent of the blade buoyancy parameter.

Paul et al. (2016) conducted drag force measurements in a large wave flume under a wide range of wave conditions, both regular and irregular. They used artificial vegetation to manipulate three parameters: stiffness, still frontal area and material volume as approximation for biomass. By varying one parameter and keeping the others constant, they studied the influence of these parameters on the drag forces. Flexible plastic strips were used as plant mimics under a range of non-breaking wave conditions and five drag sensors were installed to measure directly the drag forces in both directions (in the direction and counter to wave propagation). It showed that stiffness and the dynamic frontal area determined the drag forces and that forces do not increase linearly with increasing material volume. Short distances between the mimics could cause their interaction in cross-stream direction and result in additional drag forces. The model of Luhar et al. (2011) was used to estimate the drag forces. This model was only used for unidirectional flow, this study is the first to apply it to an oscillatory flow. The modelled drag forces were compared with the measured ones and it showed that the model was able to perform very well for both regular and irregular waves, although it yields a slight underprediction of forces. This might be due to the acceleration under waves which creates additional inertia forces. Visual observations alongside force

measurements are required to incorporate the interactions in the model. In this study, it is concluded that the force-velocity relationship depends on the vegetation stiffness (described by the flexural rigidity), rather than the biomass. In regions with low orbital velocities (still frontal area), thicker and stiffer vegetation might be more effective while in regions with higher velocities, flexible shoots might be more beneficial.

In another study (Luhar et al., 2016), which incorporates numerical modelling and laboratory experiments, the previous method is adapted for wave-induced flows. The numerical model is based on the Morison formulation of the external forces which include the net buoyancy force, the Froude-Krylov force, the drag force, the skin friction and the added mass force. As in previous studies, only individual flexible blades with uniform rectangular cross-section are considered. In the previous study, Luhar et al. (2011) demonstrated that the reconfiguration of the vegetation in unidirectional flows depends on two dimensionless parameters: the Cauchy number Ca , and the buoyancy parameter B . For wave-induced oscillatory flows, however, the Keulegan-Carpenter number, KC , and the ratio of the blade length to the wave orbital excursion, L , also play a significant role. The formulas of the different parameters are given below, with A_w the horizontal wave excursion. The velocity fields are considered oscillatory with period T_w and U_w represents the local magnitude of the horizontal wave-induced oscillatory velocity. For oscillatory flows, the drag coefficient C_D depends on KC , hence C_D is not included in the definition of Ca .

$$Ca = \frac{\rho b_s U_w^2 h_s^3}{EI}, \quad B = \frac{(\rho - \rho_s) g b_s t h_s^3}{EI}, \quad KC = \frac{U_w T_w}{b_s}, \quad L = \frac{h_s}{A_w}$$

For steady flows, the blade buoyancy delayed the onset of reconfiguration until the Cauchy number exceeded the buoyancy parameter. For oscillatory flows, however, buoyancy is only important as long as $CaL < B$. For upright blades, the contribution of the buoyancy to the blade-normal force balance is negligible.

If the drag forcing is much larger than the restoring force due to blade stiffness, $Ca \ll 1$, the blade remains nearly upright and a flat plate drag coefficient can be applied to predict the hydrodynamic drag generated by the blade. When the hydrodynamic forcing increases such that it becomes larger than the restoring force due to stiffness, $Ca > O(1)$, the blade starts to bend and move in response to the water. The resulting drag reduction depends on the ratio of the blade length to the wave orbital excursion L . For large excursions, $L \ll 1$, a quasi-steady situation arises in which the flexible blade is pushed over and remains bent until the direction of the oscillatory flow reverses. This bent posture reflects the balance between the hydrodynamic forcing and the restoring force due to stiffness. The effective lengths scales as $l_e/h_s \sim Ca^{-1/3}$, identical to the scaling for unidirectional flow. For small excursions, $L \gg 1$, the blade remains quasi vertical throughout the wave cycle. The beam equations may be linearized and the model developed by Mullarney and Henderson (2010) holds. The effective length scales as $l_e/h_s \sim (CaL)^{-1/4}$ and represents the blade length over which there is significant relative motion between the blade and the water, while the upper part moves passively with the flow. For intermediate cases with $L \sim O(1)$ the small-excursion scaling laws apply as well. The different scaling laws are presented in Figure 6.

For the scaling laws it is assumed that drag is the dominant hydrodynamic forcing. However, for wave-induced oscillatory flows, inertial effects such as added mass can also play a significant role. The added mass is expected to scale as $\rho b_s^2 U_w$ and the drag force as $\rho b_s U^2$. KC can therefore be used to estimate the relative magnitude of drag and inertial effects, as this is dimensionless parameter the ratio between the wave orbital excursion and the blade width. For the quasi steady case with large excursion, buoyancy can delay the onset of reconfiguration, as was the case for a steady flow. However, in the small-excursion case, buoyancy will not likely have influence.

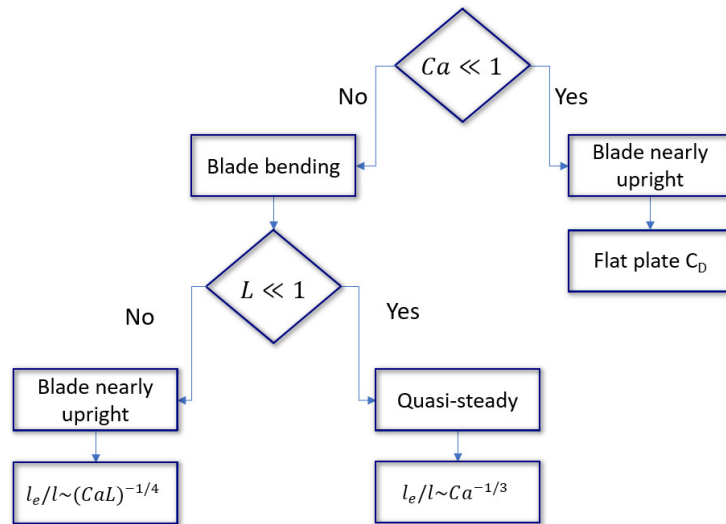


Figure 6: Scaling laws for wave-induced flows

The experimental tests involved two distinctive blade materials (silicon foam and high-density polyethylene), representing two different species, with four different blade lengths, subjected to eight various wave conditions. The numerical model adequately predicted the forces generated by the model blades over the range of wave conditions tested in the laboratory, however, there are significant differences between the measured and predicted blade postures for the highly flexible foam blades, especially near the tip of the blade. The causes of these discrepancies may be the assumption that the drag coefficient C_D and the added mass coefficient C_M are constant over the entire blade length, which are in reality reduced towards the blade tip, and the twisting of the foam blades near the tip that is not taken into account in the model.

Summarized, the effective blade length depends on two important dimensionless parameters: (i) the Cauchy number Ca and (ii) the ratio of the blade length to the wave orbital excursion L . The framework for individual blades adequately accounts for the effect of blade motion on wave decay at the canopy-scale. Luhar et al. (2016) suggest to reanalyse the existing datasets on wave attenuation as a first step to implement a general framework. The concept of effective length should be applied to these datasets and the variation of it with respect to the parameters Ca , B , and L should be investigated. Care should be taken considering the way the effective length is defined. This may become complicated if the wave-induced flow varies significantly over the depth and this may depend on the focus of the study, either drag reduction or wave energy dissipation.

Luhar et al. (2017) investigated the impact of seagrass blade motion on wave decay and identified a scaling law that predicts wave decay of the model meadow over a range of stem densities, wave periods, wave heights and water depths. In the current laboratory study the seagrass *Zostera marina* is mimicked by a submerged flexible mimic and the blade posture and motion is observed over the entire length of the blade to investigate the vertical distribution of wave drag. The model developed by Dalrymple et al. (1984) is used to analyse wave decay, which uses the dimensionless parameter $K_{D0}\lambda$, as explained previously. The principle of effective blade length is applied to this model, by replacing the total length of the blade l by the effective length l_e , to quantify the impact of blade motion on wave decay. As shown in the previous study (Luhar et al. 2016), the effective length depends primarily on two dimensionless parameters: (i) the Cauchy number Ca and (ii) the ratio of the blade length to the orbital wave excursion L .

For the laboratory experiments, mimics are fabricated from low-density polyethylene (LDPE). With a Cauchy number $Ca \geq 100$ and a ratio of blade length to wave excursion $L \geq 2.7$, high forcing that causes bending is expected ($Ca \gg 1$) together with small excursions ($L \gg 1$). For this case, the effective length scales to $l_e/h_s \sim [CaL]^{-1/4}$. The impact of vegetation

characteristics (stem density and submergence ratio) and wave properties (wave period and wave amplitude) on wave attenuation was investigated. It was found that wave attenuation increased with increasing vegetation density, with increasing wave period and with higher wave heights, as well as for meadows that occupied a larger fraction of the water column. The blade motion from the video analysis agrees well with the expected scaling law, with a best fit to the data for $l_e/h_s = 2.25(CaL)^{-1/4}$. The accuracy of the effective length concept was proven by comparing the predicted wave attenuation to the observed wave decay. The wave decay was first predicted with the assumption of rigid blades ($l_e = l$), which resulted in an overprediction of 350%. Compared to an overprediction of 8% for the effective length $l_e/h_s = 2.25(CaL)^{-1/4}$. With this method, the effects of vegetation bending and motion can be incorporated in the effective length, depending primarily on the Cauchy number Ca and the length ratio L . The effects of shape and Reynolds number, on the other hand, can be accounted for by the drag coefficient C_D .

Möller et al. (2014) have investigated the effectiveness of wave attenuation under extreme conditions, when water levels are maximum and waves are highest by conducting laboratory experiments on a transplanted section of natural salt marsh. They found that the vegetation causes considerable wave attenuation: up to 60% of observed wave reduction was attributed to vegetation. Tests were conducted for regular and irregular non-breaking waves with a wave height up to 0.9 m in 2m water depth above the vegetated bed. For regular waves with wave height larger than 0.3 m, the wave dissipation was reduced due to a change in behaviour of the vegetation. Under relatively low incident waves, the plants swayed and interacted with wave motion. For larger waves, the stem bent over to angles larger than 50° during the forward wave motion, allowing the flow to skim over, instead over travel through the vegetation.

Influence of blade flexibility on C_D

The assumption that aquatic vegetation is rigid, overestimates highly the ability to attenuate waves. However, assuming that the vegetation is fully flexible, underestimated the wave attenuation. Houser et al. (2015) studied quantitatively the influence of blade flexibility on the drag coefficient C_D of aquatic vegetation. They conducted laboratory experiments over a range of water depths and wave conditions with four artificial, submerged vegetation mimics of varying rigidity, amongst which two flexible mimics (cable ties and ribbon) and two rigid ones (flexible and inflexible balsa wood dowels). The results are compared to previous C_D - Re relationships from field, laboratory and numerical modelling studies, represented in Table 1. The flexible vegetation data exhibited a similar relationship between C_D and Re . The rigid vegetation data could be approximated by the non-swaying model of Mendez et al. (1999). For the semi-flexible vegetation the relationship is more complex and depends on the submergence ratio. The model of Kobayashi et al. (1993) and the model of Mendez et al. (1999) for flexible vegetation can be used as an approximation. The similarity of these relationship suggests that models are using an appropriate formalization of blade flexibility or lack thereof.

Houser et al. (2015) concluded that the drag coefficient and the ability to attenuate waves depend strongly on the flexibility of the individual blades. This study is the first to examine how the C_D varies with the flexibility of a blade that is morphologically and dynamically similar to *T. testudinum*. The C_D exhibits a statistically significant dependence on the rigidity parameter λ_1 (Ghisalberti and Nepf, 2002), which suggests that the rigidity parameter can be used to estimate the wave attenuation by vegetation for a given blade morphology and canopy structure using simple design variables from the prototype.

In previous studies the drag coefficient C_D has been predicted by relating it to a Keulegan-Carpenter (KC) number, originally used in coastal engineering literature where it is used to predict drag on piles. For a rigid cylinder, this method is accurate but not for flexible aquatic vegetation for three reasons. The frontal area of the blade is reduced because of the bending, the relative velocity between the blade and the fluid is altered because of the movement, and the grouping of elements into canopies results in reduced wave velocities. Therefore, Zeller et al. (2014) introduced an alternative KC number where

the horizontal excursion of the blade tip is used as length scale for the vegetation, instead of the width of the blade. This KC takes the bending of the blade into account and turned out to be a better predictor for the drag coefficient.

To predict wave attenuation based on the KC requires extensive measurements of vegetation properties. The model developed here, with adjustable parameters, is more practical to study the influence of physical parameters. The model is validated by laboratory experiments in the wave flume with an underlying current. Four different single-blade mimics were constructed from rigid low-density polyethylene (LDPE) rectangular plates, attached to torsion springs at the joints. These torsion springs account for the rigidity of the blade. The numerical model predicted the blade tip movement perfectly, compared to the results from the laboratory experiments and the adapted Keulegan Carpenter number is an excellent predictor of the drag coefficient. For a small KC, the blade pronates late in the wave phase and the fluid encounters most of the blade's frontal area. Hence the drag coefficient will be high. This indicates the inverse relationship between the drag coefficient and the KC. Zeller et al. (2014) only used an individual blade instead of a full canopy, which implies a different behaviour. Due to the velocity reduction in the canopy and the physical interaction between the blades, the effective rigidity increases. The model could be adjusted to mimic the blade motion and wave attenuation in a canopy.

Parameters influencing the wave attenuation by vegetation

Wave attenuation by vegetation depends on the vegetation characteristics such as geometry, buoyancy, density, stiffness and spatial coverage, as well as on the wave conditions like wave height, period and direction (Anderson et al., 2011).

Vegetation properties

Stiffness

Fonseca and Cahalan (1992) discovered that differences in flexibility and streamlining may reduce the stress on the vegetation, by reducing the frontal area exposed to the flow. A comparative study between stiff salt marsh vegetation and flexible seagrass indicated that plant stiffness influences the wave attenuation with stiffer vegetation being more effective at reducing wave energy. This was confirmed by Koehl (1996) and Denny et al. (2002). Bouma et al. (2005) also compared the wave attenuation capacity of two artificial mimics with contrasting stiffness and found that the wave dissipation for the stiff mimics was a factor three higher compared to the one for the flexible mimics. The drag force, measured by force transducers, was highest and most sensitive to hydrodynamic forces in stiff vegetation. The flexible vegetation avoided part of the drag by bending, also called reconfiguration. They concluded that the vegetation stiffness determines both the capacity to reduce wave energy and the drag that needs to be resisted.

However, when comparing a mimic exhibiting cantilever motion to rigid structures, the effect of stiffness was not encountered and both rigid and flexible vegetation yielded the same friction factors (Augustin et al., 2009).

Mullarney and Henderson (2010) found an increasing dissipation with increasing stiffness, depending on the frequency, as was found by Bradley and Houser (2009). High and low frequency waves are preferentially damped, while the intermediate frequencies could pass easily. This is confirmed by Anderson et al. (2014) for mimics of cross linked polyolefin (XLPO) tubing and irregular waves.

Depending on their stiffness and length, seagrasses can move in a cantilever or a whip-like motion. A transition between both can be observed when the wave forcing is increased (Manca, 2010). Paul et al. (2012) used two artificial mimics with different flexibilities to simulate *Z. noltii*: stiffer cable ties which behave like a cantilever and flexible poly ribbon which shows the typical whip-like motion of seagrasses for longer leaf lengths. For the stiffer material a 4 times higher wave attenuation was obtained compared to the flexible material. However, the reduced attenuation of flexible plants can be counteracted by a higher shoot density, which was also found by Bouma et al. (2010). According to Houser et al. (2015) the drag depends on whether the oscillatory velocity is able to overcome the rigidity of the vegetation. An increase in flexibility

is in general associated with a reduced ability for wave attenuation. Dijkstra and Uittenbogaard (2010) observed a more upright position of the blade for stiffer plants and an increased drag.

Submergence ratio

Due to the wave horizontal orbital velocities being highest near the crest of the wave and decreasing towards the bed, it is expected that the wave attenuation increasing with increasing submergence ratio. The latter is defined as the ratio of the vegetation height to the water depth h_v/h . When the vegetation becomes emergent, the entire velocity profile is impeded, compared to submerged conditions where the highest orbital velocities pass over the meadow, as shown in Figure 7. Therefore, the wave attenuation is expected to be higher for emergent conditions (Anderson et al., 2011).

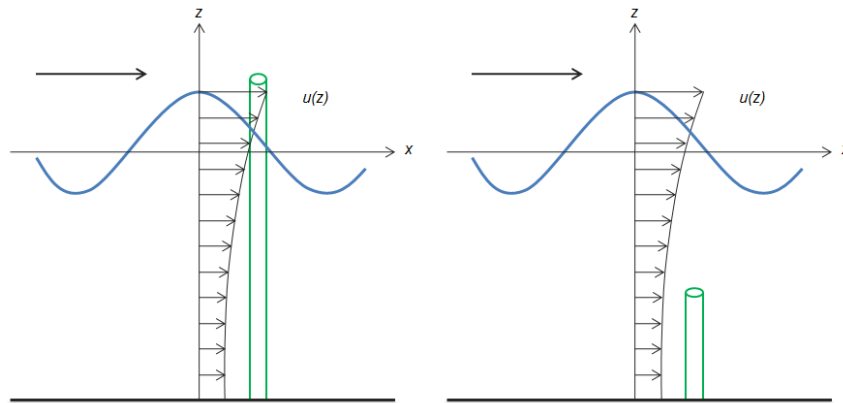


Figure 7: Interactions of particle velocities with emergent (left) and submerged (right) stems. (Anderson et al., 2011)

Early studies (Ward et al. 1984, Fonseca et al. 1992, Koch 1996) found that the wave attenuation-capacity of seagrass increases when it occupies more of the water column. This confirmed that wave attenuation decreases with decreasing submergence ratio, which is also found by Mendez and Losada (2004), Chen et al. (2007), Stratigaki et al. (2011), Koftis et al. (2013), Luhar et al. (2017) and Anderson et al. (2014). Augustin et al. (2009), Dubi and Tørum (1996) and Fonseca and Cahalan (1992) and later Maza et al. (2016) found that wave attenuation was higher for emergent conditions, which is most widely found for wetlands, because the vegetation occupies the entire water column. For near-emergent conditions, wave attenuation was mostly dependent on the submergence ratio of the vegetation. This is confirmed by Houser et al. (2015) who found that for semi-flexible vegetation, the drag increases significantly when the vegetation is submerged, compared to the emerged case. The drag coefficient decreases with further decreasing the submergence ratio, due to the larger velocities at the free surface. When the submergence ratio decreases, the drag force will decrease in response to the smaller velocities. This was found earlier by Hu et al. (2014) for stiff wooden rods.

Paul et al. (2012) studied the effect of leaf length on the ability of vegetation to attenuate waves. Unlike other studies, they used a constant water depth and varying leaf lengths (three) to simulate different submergence ratios. This way, the wave parameters are constant and cannot influence the results. They found no significant effect of the submergence ratio on wave height dissipation, which might be due to the experimental setup. By altering the length of the vegetation, LAI increases with increasing submergence ratio for a given shoot density. With LAI the dominant influencing parameter, it may have affected the relationship between the submergence ratio and the dissipated wave height. Although not significant, the wave attenuation increased with decreasing submergence ratio while the influence of the shoot density decreased.

Dijkstra and Uittenbogaard (2010) found an increased bending for longer plants, while shorter plants remained almost upright and experienced more drag. For increasing water depths, the bending and the effect on the flow decreased.

Shoot density

As discussed earlier, wave attenuation will be higher when the vegetation takes up more of the water column. Hence, it is expected to increase with increasing shoot density.

Dubi and Torum (1997) found that the damping coefficient increased with increasing shoot density until it reached a maximum, after which it decreased sharply with increasing density. Bouma et al. (2005) used artificial mimics of *Zostera* and *Spartina* in flume experiments and found for both mimics an increased wave height dissipation with increasing shoot density. This confirmed the results of Fonseca and Cahalan (1992), who stated, however, that the shoot density is not more influential than other potentially important factors such as the morphology and flexibility of the plant. A higher wave attenuation with increasing shoot density was obtained for stiff wooden rods (Hu et al., 2014), as well as for polypropylene (Stratigaki et al., 2011; Koftis et al., 2013) and low-density polyethylene mimics (Luhar et al., 2017) and cross linked polyolefin (XLPO) tubing (Anderson et al., 2014). This is consistent with the results of Mendez and Losada (2004) and Chen et al. (2007).

Dijkstra and Uittenbogaard (2010) observed a more upright blade position and a distinctly different flow profile when the number of plants increases.

Leaf Area Index (LAI)

Unlike other studies, Paul et al. (2012) used a larger number of different shoot densities (5) to further investigate the relationship between shoot density and wave attenuation. They combined the effects of shoot density and leaf length in the parameter LAI (Leaf Area Index), which is the product of the leaf length, leaf width and shoot density, and identified this parameter to be the dominant one. They found a linearly increasing relationship between the dissipated wave height and LAI, with a significantly higher slope for the stiffer material. This suggests that the wave attenuation of a short but dense meadow is the same for a high but sparse meadow with the same LAI. However, it is likely that this conclusion only holds for shallow wave conditions where the waves feel the bottom. For conditions with the orbital wave motion not reaching the bottom, a higher meadow is expected to yield a higher attenuation.

Hydrodynamic conditions

Wave period

The effect of wave period on wave attenuation is the most contradictory and unresolved. It is expected that attenuation is higher in shallow water (with longer wavelengths and higher wave periods) because the orbital velocities are higher in this case. For shallow water waves, the horizontal excursion is constant over the depth, whereas it decays exponentially from the surface towards the bed for deep water waves, as shown in (Anderson et al., 2011).

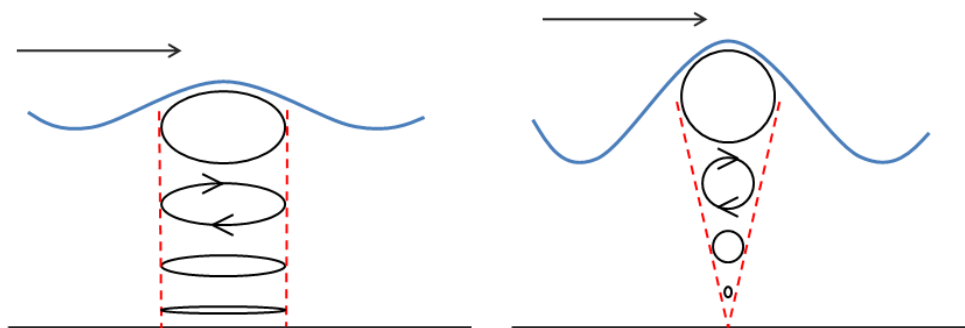


Figure 8: Particle trajectories for shallow water (left) and deep water (right) waves. (Dean and Dalrymple, 1991)

Möller et al. (1999) found a reduction of wave energy for all frequencies by the same degree. Bradley et al. (2009) and Lowe et al. (2007) stated that the seagrass also acts like a low-pass filter that dissipates higher frequency components

more effectively. Longer waves, with larger wave periods, are found to be mostly attenuated by Cavallaro et al. (2010), Fonseca and Cahalan (1992), Koftis et al. (2013) and Maza et al. (2016). Sánchez-González et al. (2011) obtained a higher attenuation for steeper waves, with the steepness H/λ increasing with decreasing wave period. On the contrary, John et al. (2016) and Luhar et al. (2017) obtained an increased wave attenuation with increasing wave period and decreasing wave steepness.

Wave height attenuation is found to be more substantial in shallow water, compared to deep water, by Dubi and Torum (1997). They found an increase of the wave attenuation with increasing wave period, until it reached a maximum, after which it decreased gradually with the wave period. The experimental damping coefficient varies more widely for shorter peak periods, for longer peak periods it is almost independent of the peak period and nearly converges.

Wave height

When the wave height increases, the drag force on the vegetation will increase and hence the wave attenuation by vegetation is expected to be higher for higher wave forcing.

From the results of Asano et al. (1992), it showed that the damping coefficient increased with the wave amplitude, which yields a higher attenuation. This is confirmed by Chen et al. (2007), Luhar et al. (2017) and John et al. (2016) for flexible mimics. For the tests of Anderson et al. (2014) increasing the wave height slightly increased the attenuation, mostly in shallower water. Maza et al. (2016) confirmed the higher attenuation for larger wave heights, with a linear fitting for emergent conditions. For submerged conditions a different relationship is found.

Tidal current

Li and Yan (2007) were the first to investigate wave dissipation by vegetation in the presence of a following current, i.e. in the direction of wave propagation. They concluded that following currents enhance the ability of vegetation to attenuate waves. Paul et al. (2012), however, found that the dissipated wave height decreased significantly for combined wave-current conditions compared to pure wave conditions. The result was even found for control runs without vegetation. This is explained by the Doppler effect that arises when a following current is combined with waves, which yields a higher wavelength, and Nielsen (1992) observed that wave attenuation is lower for higher wavelengths. The effect was especially noticeable for high shoot densities. Furthermore, it was noticed that the tip excursion of the leaves reduced in the presence of the current. They concluded that studying wave attenuation under pure wave conditions generates a structural overestimation of the wave-attenuation capacity of seagrass compared to most natural environments with underlying currents.

Hu et al. (2014) assessed the effect of tidal currents and showed that the contradictory results from Li and Yan (2007) and Paul et al. (2012) may be caused by a difference in ratio of imposed current velocity U_c to amplitude of the horizontal wave orbital velocity U_w . For a small value of this ratio, the wave dissipation decreases when adding an underlying current to incident wave conditions. The opposite holds for large values of the ratio: the wave dissipation is increased. The wave dissipation is influenced for all the tests, except for the tests at the transition points, for which the wave dissipation is the same as it is in pure wave conditions. As Paul et al. (2012) performed tests with relatively small values of the ratio and Li and Yang (2007) applied large values, the contradictive conclusions can be explained.

Chapter 3: Mimics of *Posidonia oceanica*

The adoption of mimics

Utilizing real seagrasses in the laboratory induces multiple practical complications. Above all, the seagrass cannot be taken from the field as it is a protected species and the growth of large numbers of plants requires a substantial amount of time and effort to ensure that the plants embody the required properties. Furthermore, the plants cannot be stored in between two testing periods and therefore cannot be reused. Additionally, the plants need to maintain their properties throughout the entire testing period to ensure the reliability of the experiment results. Even with persistent attention to the laboratory, water and nutrient conditions, it is doubtful that the plants will exhibit their original characteristics.

To eliminate the aforementioned complications, artificial plants or mimics are fabricated which can be used in the laboratory. These mimics are reusable and sustainable, and can be produced in large numbers for a competitive price. The mimics have the simple leaf geometry of the proposed vegetation along with the required characteristics. This way, a large meadow can be constructed with homogeneous plant properties.

Previously used mimics

A number of researches have conducted experiments with the use of mimics, with various materials, geometries and scaling factors. Table 2 gives an overview of the element types and vegetation of interest for known laboratory studies of wave attenuation through vegetation and is an extension of the summary given by Anderson et al. (2013). This overview is used as a source of inspiration to find a suitable material for the mimics used in this study.

Table 2: Mimic materials used by several researchers to simulate different plant species

Study	Element	Plant species
Anderson et al. (2013)	Cross linked polyolefin tubing	<i>S. alterniflora</i>
Augustin et al. (2009)	Wooden dowels and polyethylene foam tubing	<i>S. alterniflora</i>
Bouma et al. (2005), Paul et al. (2012)	Tie wraps and poly ribbon	<i>S. anglica</i> and <i>Z. noltii</i>
Cavallaro (2010), Maltese et al. (2007)	Polyethylene	<i>Posidonia oceanica</i>
Dubi and Tørum (1996), Løvas and Tørum (2000)	Moulded plastic	<i>L. hyperborea</i>
Elginos et al. (2011)	Nickel-chrome wire	<i>Posidonia oceanica</i>
Folkard (2005)	Polyethylene sheeting	<i>Posidonia oceanica</i>
Fonseca and Cahalan (1992)	Real plants	<i>H. wrightii</i> , <i>S. filiforme</i> , <i>T. testudinum</i> , <i>Z. marina</i>
Fonseca and Koehl (2005)	Polypropylene ribbon	<i>Z. marina</i>
Ghisalberti and Nepf (2002), Luhar et al. (2010), Luhar et al. (2017)	Polyethylene film	<i>Z. marina</i>
Houser et al. (2015)	Wooden dowels, tie wraps and ribbon	<i>T. testudinum</i>
Hu et al. (2014)	Wooden rods	Not specified
Koftis et al. (2013), Manca et al. (2012), Stratigaki et al. (2011)	Polypropylene stripes	<i>Posidonia oceanica</i>
Li and Yan (2007)	Rubber rods	Not specified
Lima et al. (2006)	Nylon rope	<i>B. subquadripara</i>
Mei et al. (2011)	Perspex cylinders	Not specified
Ota et al. (2004)	Polyester bands	Not specified
Sánchez-González et al. (2011)	Polyethylene and polypropylene	<i>Posidonia oceanica</i>
Tschirky et al. (2000)	Real plants	<i>Scirpus Validus</i>

Design of the mimics

The non-dimensional parameters for the design of the mimics are the mass ratio, the slenderness number and the Cauchy number (Stratigaki et al., 2011):

$$M = \rho/\rho_s$$
$$S = L/l$$
$$Ca = \frac{\rho U^2 S^3}{E}$$

with L and l the maximum and minimum cross-sectional dimensions of the plant, respectively the plant height and width, and U the characteristic velocity. Luhar et al. (2017) defined a slightly different Cauchy number, which will be used here:

$$Ca = \frac{\rho b_s U^2 h_s^3}{EI}$$

According to Ghisalberti and Nepf (2002), the blade movement is determined by the drag force (F_D) and the restoring forces due to the buoyancy (F_B) and the rigidity (F_R) of the leaves. The inertial term due to the accelerating fluid is neglected because of the small width of the blades. Two non-dimensional scaling parameters can be matched between the model and the prototype to design the seagrass mimics and obtain dynamic similarity. λ_1 is the ratio of the blade buoyancy over the blade rigidity and λ_2 is the ratio between the blade rigidity and the drag force:

$$\lambda_1 = \frac{F_B}{F_R} = \frac{(\rho - \rho_s)h_s^3}{Et^2}$$
$$\lambda_2 = \frac{F_R}{F_D} = \frac{Et^3}{h_s^3 U_c^2}$$

With ρ_s and ρ the solid density of the blades and the fluid density respectively and U_c the mean in-canopy velocity. To assure dynamic similarity, both scaling parameters need to be equal for the model and the prototype. This way the whip-like motion of the leaves is accurately modelled.

Further elaboration of the previous formulas by considering Froude scaling, as done by Sanchez-Gonzalez et al. (2011), results in the following scaling law

$$E_p = N_L \cdot E_m \cdot \frac{(\rho - \rho_s)_p}{(\rho - \rho_s)_m}$$

with m and p subscripts for model and prototype and in which N_L represents the scale factor L_p/L_m .

Posidonia oceanica properties

For the current experiments, the proposed vegetation is *Posidonia oceanica* due to its simple leaf geometry and its importance in the Mediterranean Sea. *Posidonia oceanica* is one of the most abundant species of seagrasses endemic to the Mediterranean Sea, covering about 1.5% of the total Mediterranean Sea surface and occurring in 16 Mediterranean countries (Vacchi et al., 2017). It is present along almost all coasts, avoiding estuaries where the input of freshwater and fine sediment is high. Figure 9 shows the distribution of *P. oceanica* within the Mediterranean Sea. It can form continuous meadows or it can be organized in patches, occurring from near the surface up till 40-50 m depth, with sand as common substrate but also attaching to rocks and coralligenous formations. The beds of *P. oceanica* are among the most important Mediterranean ecosystems, making their conservation an international priority, hence they are protected by several

European Union directives and national laws. Photographs of *Posidonia oceanica* meadows are given in Figure 12, made by M. San Félix and retrieved from Arnaud-Haond et al. (2012).



Figure 9: Distribution of *Posidonia Oceanica* in the Mediterranean Sea (Vacchi et al., 2017)

A typical plant of *P. oceanica*, as shown in Figure 10, consists of an above-ground, visible part with linear leaves that is attached to rhizomes within or on top of the sediment from which roots penetrate into deeper layers (Borum et al., 2004). It consists of an alternating arrangement of leaves, with the youngest leaves (< 5 cm) at the centre of the shoot and the oldest ones on the outside. The growth of alternating horizontal and vertical rhizomes and the slow decay of this material, causes *P. oceanica* to form a typical terraced formation called “matte”. It can rise up to a few meters and can be thousands of years old, consisting of roots, rhizomes and entangled sediment. The properties of a common *P. oceanica* plant can be found in Table 3, for both deep and shallow water conditions (Buia, 2004).

Table 3: Properties of *Posidonia oceanica*

	Leaves/shoot	Max. length leaves h_s [cm]	Max. width leaves b_s [cm]	Rhizome diameter [mm]	Shoot density [shoots/m ²]
Shallow	8	75	1.25	10	700
Deep	7	69	1	10	161

Folkard (2005) measured the leaf thickness, the density and modulus of elasticity of natural *P. oceanica*, which will determine the oscillatory motion of the vegetation. The obtained values are presented in Table 4.

Table 4: Mechanical properties of *Posidonia oceanica*

Modulus of elasticity E [GPa]	Solid density ρ [kg/m ³]	Leaf thickness t [mm]
0.41 – 0.53	800 – 1020	0.2



Figure 10: *P. oceanica* plant with distinct, broad leaves and hairy remains around rhizomes (Borum et al., 2004)

Mimics selection and configuration

For the experiments in this study, each mimic consists of one flexible blade, attached to a rigid cylinder which represents the lower, stiff stem of the seagrass. The cylinders are hollow with a diameter of 2 cm, protruding 1.5 cm above the board and made from PVC. The leaves are made from different flexible materials and all strips have a width of 1 cm to be able to get a useful reading from the drag sensors. The strips are clamped in the cylinders by a silicone, conical stopper. The design of the mimic is depicted in Figure 11.

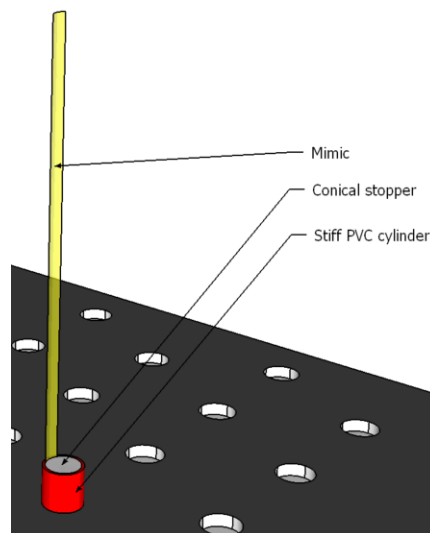


Figure 11: Mimic design

The blades are fabricated from strips of three different materials to study the influence of stiffness on wave attenuation. The first mimics are cut from the covers of notebooks (Atoma), the second type of mimics is cut from the lids of plastic pots and the third mimics are cable ties. The cable ties are manufactured from polyamide, also known under the brand name of nylon, and the other two mimics from polypropylene. However, because the two mimics have a different thickness, the flexural rigidity (i.e. the product of the elasticity modulus E and the second moment of area I) will be different for all three materials. These materials are chosen because they have similar properties compared to real *Posidonia oceanica*

leaves, which have a density of 800 - 1020 kg/m³, a Young's modulus of 0.41 - 0.53 GPa and a thickness of 0.2 mm (Buia, 2004). The mimics are not intended to offer a perfect model for the plant species and do not attempt to perfectly reflect all characteristics of *Posidonia oceanica* (e.g., the cable ties have small ripples on the downstream side instead of being perfectly flat). However, these kind of deviations are of relatively minor importance when trying to obtain a general insight in the behaviour of vegetation under wave forcing (Bouma et al., 2005).

To be able to study the influence of stiffness on wave attenuation, an estimate of the overall flexural stiffness for the different materials needs to be known. The thickness of the strips is determined by measuring the total thickness of a bunch of strips and dividing it by the number of strips. As the width of the mimics is known, the second moment of inertia I can be calculated

$$I = \frac{b_s t^3}{12}$$

with b and t the width and thickness of the leaves respectively.

The density and the modulus of elasticity are not specified by the manufacturer, but the types of the materials are known and based on Bashford (1996), Mark (1998) and previously used mimics, an estimation can be made on the properties of the different materials. An overview of the mimics and their properties is presented in Table 5.

Table 5: Mechanical properties of the mimics compared to real P. oceanica

	Product	Material	Young's modulus (E)	Density (ρ)	Thickness (t)	Second moment of area (I)	Flexural rigidity (EI)
			[GPa]	[kg/m ³]	[mm]	[m ⁴]	[Nm ²]
Mimic 1	Notebook cover	Poly-propylene	0.90 – 1.60	880 - 920	0.500 (± 0.019)	$1.04 (\pm 0.12) \times 10^{-15}$	$(8.37 - 18.6) \times 10^{-14}$
Mimic 2	Lid	Poly-propylene	0.90 – 1.60	880 - 920	0.250 (± 0.008)	$1.30 (\pm 0.13) \times 10^{-14}$	$(1.07 - 2.28) \times 10^{-14}$
Mimic 3	Cable ties	Polyamide (nylon)	2.00 – 3.20	1070 - 1140	1.57 (± 0.04)	$2.91 (\pm 0.20) \times 10^{-12}$	$(5.43 - 9.96) \times 10^{-12}$
P. oceanica			0.41 – 0.53	800 - 1020	0.2	6.67×10^{-15}	$(2.73 - 3.53) \times 10^{-15}$

The mimics are stiffer compared to the real *Posidonia oceanica* seagrass, i.e. the flexural rigidity is higher. Mimic 2 is the most flexible and its flexural rigidity approaches the one of the natural vegetation.

Table 6 shows the dimensionless parameters as defined previously. For mimic 2, the dynamic similarity parameter λ_1 and mass ratio M lie within the range of values of the prototype, and the Cauchy number approximates the one of the real vegetation. Hence, mimic 2 is the most suitable material to represent *P. oceanica*, followed by mimic 1. Due to the large modulus of elasticity and density of mimic 3, the ranges are less compatible between mimic 3 and the prototype.

Table 6: Dimensionless parameters of the mimics compared to real P. oceanica

	Dynamic similarity param. (λ_1)	Mass ratio (M)	Cauchy number (Ca)
Mimic 1	$(0.19 - 0.58) h_s^3$	1.087 – 1.136	$(5.38 - 11.9) \times 10^4 U^2 h_s^3$
Mimic 2	$(0.75 - 2.27) h_s^3$	1.087 – 1.136	$(4.38 - 9.39) \times 10^5 U^2 h_s^3$
Mimic 3	$-(0.002 - 0.02) h_s^3$	0.877 – 0.990	$(9.03 - 16.6) \times 10^2 U^2 h_s^3$
P. oceanica	$(0.23 - 13.7) h_s^3$	1.005 – 1.281	$(2.90 - 3.75) \times 10^6 U^2 h_s^3$



Figure 12: Photographs of meadows of P. oceanica. (Top) illustrating the individual shoots and (Bottom) an overview of the meadow.

Chapter 4: Experiment

Physical tests are conducted on a patch of mimics, representing *Posidonia oceanica* seagrass, in the small wave flume of the Department of Civil Engineering. The influence of wave conditions (wave height and wave period) and meadow characteristics (flexural rigidity and submergence ratio) on wave attenuation are studied by measuring the drag force on the blades, the wave height decay and the bending angle of the blades.

Set-up

The physical wave flume has a length, width and height of 15.0 m, 0.35 m and 0.60 m respectively, with a design water depth of 0.30 m and a maximum wave height of 0.20 m. A piston type wave paddle generates the waves with a maximum stroke of 0.40 m. The wave flume is equipped with an active wave absorption system (AWASYS) that allows the wave paddle to simultaneously generate the incident waves and absorb the spurious reflected waves.

A patch of 91 mimics is constructed on a PVC plate of 35 cm wide and 70 cm long, as illustrated in Figure 13, yielding a shoot density of 371 shoots/m². The mimics are inserted in the board in a staggered way to avoid straight lines and thus preferential flow paths through the meadow, with their width perpendicular to the flow. The board is raised approximately 10 cm above the flume bottom, simulating the tendency of *P. oceanica* to grow on a layer of mat and allowing the force transducers to fit under the board. To prevent edge effects, the board is extended 2 m backwards and 2.5 m forwards with a slope in front. A parabolic beach is placed at the end of the flume to minimize wave reflection.

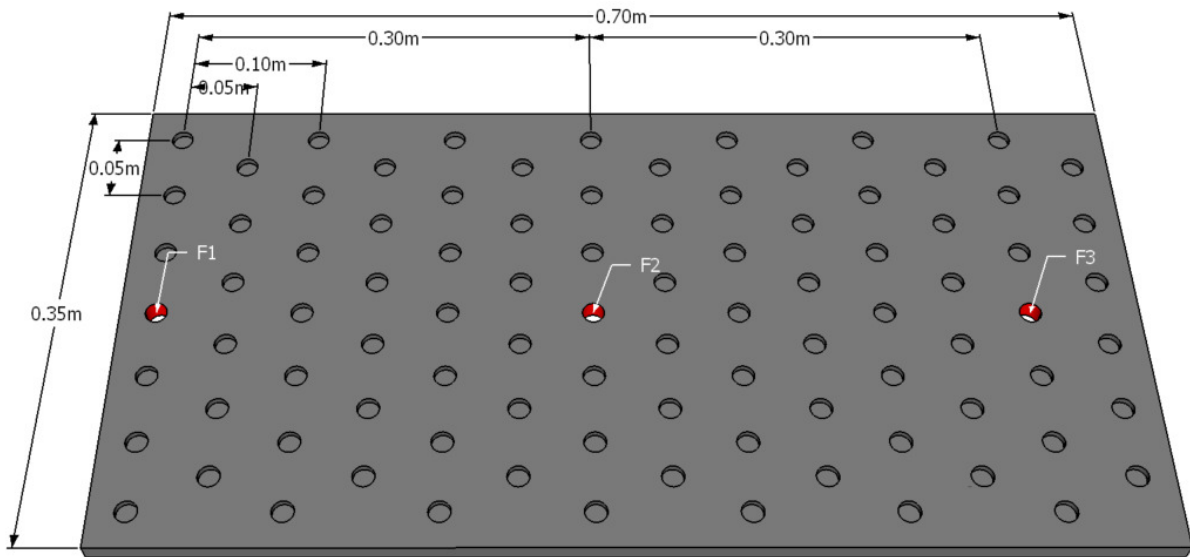


Figure 13: Mimic configuration in PVC board with positions of force transducers indicated in red

Test cases

In the present experiments, regular wave conditions based on Luhar et al. (2016) and Luhar et al. (2017) are applied, with a total of 25 different wave conditions.

Luhar et al. (2016) carried out an experimental study to investigate the motion of flexible blades, scaled to be dynamically similar to natural aquatic vegetation, under wave-induced oscillatory flows. They tested mimics made of two different materials: high-density polyethylene en silicon foam, both with a blade width of 2.0 cm and lengths varying from 5 to 20 cm. Eight different regular wave conditions were imposed on the mimics, with wave periods T ranging from 1.1 to 2.0 s and wave heights H varying between 2.0 and 8.0 cm in a water depth of 38 cm. In a later study, Luhar et al. (2017) tested mimics made from low-density polyethylene with a blade width b_v of 3 mm and a length l_v of 13 cm in water depths of 16 to 39

cm. Wave period ranged from 0.8 to 2.0 s and wave height varied between 1.8 and 11.2 cm. These values represent the shallow region of a seagrass meadow with h/λ ranging from 0.10 to 0.43 and L_w/h ranging from 0.3 to 0.8.

For the experiments of this thesis, the overall water depth h is held constant at 32 cm, which yields a water depth of 22 cm at the location of the vegetation because of the elevated position of the board. According to Koch et al. (2006), most waves in seagrass beds are intermediary ($0.04 < h/\lambda < 0.5$) so the range of waves tested here ($0.10 < h/\lambda < 0.27$) complies with natural conditions for seagrass. Due to the foreland, some shoaling of the waves will occur which slightly increases the wave height and decreases the wave length to some extent. However, because this effect is the same for all test conditions and this paper focuses on the relative differences between the various test cases, the shoaling is not taken into account. An overview of the wave conditions is given in Table 7.

Table 7: Wave conditions

Test nr	Wave period T [s]	Wave height H [m]	Wave length λ [m]	Dispersion parameter h/λ [-]	Wave steepness H/ λ [-]	Wave number k [1/m]
01	0.9	0.02	1.183	0.27	0.02	5.310
02	0.9	0.04	1.183	0.27	0.03	5.310
03	0.9	0.06	1.183	0.27	0.05	5.310
04	0.9	0.08	1.183	0.27	0.07	5.310
21	0.9	0.10	1.183	0.27	0.08	5.310
05	1.1	0.02	1.604	0.20	0.01	3.916
06	1.1	0.04	1.604	0.20	0.02	3.916
07	1.1	0.06	1.604	0.20	0.04	3.916
08	1.1	0.08	1.604	0.20	0.05	3.916
22	1.1	0.10	1.604	0.20	0.06	3.916
09	1.4	0.02	2.208	0.14	0.01	2.845
10	1.4	0.04	2.208	0.14	0.02	2.845
11	1.4	0.06	2.208	0.14	0.03	2.845
12	1.4	0.08	2.208	0.14	0.04	2.845
23	1.4	0.10	2.208	0.14	0.05	2.845
13	1.7	0.02	2.788	0.11	0.01	2.254
14	1.7	0.04	2.788	0.11	0.01	2.254
15	1.7	0.06	2.788	0.11	0.02	2.254
16	1.7	0.08	2.788	0.11	0.03	2.254
24	1.7	0.10	2.788	0.11	0.04	2.254
17	2.0	0.02	3.353	0.10	0.01	1.874
18	2.0	0.04	3.353	0.10	0.01	1.874
19	2.0	0.06	3.353	0.10	0.02	1.874
20	2.0	0.08	3.353	0.10	0.02	1.874
25	2.0	0.10	3.353	0.10	0.03	1.874

To investigate the influence of submergence ratio on wave attenuation, different submergence ratios are tested. The submergence ratio can be changed either by varying the water depth or alternatively by altering the height of the vegetation. The latter is the best option as this retains the same wave conditions over all the tests and hence does not induce any effects that could influence the tests. For mimics 1 and 3, the 25 tests are carried out for three different

vegetation lengths (20, 16 and 13 cm including the height of the stiff base of 1.5 cm). Mimic 2 does not exist for the largest length and is only tested for the remaining two lengths (16 and 13 cm).

All of the above leads to a total of 200 tests. A_i , B_i and C_i denote the test conditions for mimic 1 with i ranging from 1 to 25 and the lengths of the mimics being reduced in between each of the three series from 20 to 16 cm and subsequently to 13 cm. Similarly, D_i and E_i represent the conditions for mimic 2 with blade lengths of 16 and 13 cm respectively. Likewise, F_i , G_i and H_i stand for the conditions for mimic 3. An overview of the test conditions is given in Table 8.

Table 8: Test conditions

	Seagrass height h_s [m]	Submergence ratio h_s/h [-]	Test codes
Mimic 1	0.20	0.91	A01-A025
	0.16	0.73	B01-B025
	0.13	0.59	C01-C025
Mimic 2	0.16	0.73	D01-D025
	0.13	0.59	E01-E025
Mimic 3	0.20	0.91	F01-F025
	0.16	0.73	G01-G025
	0.13	0.59	H01-H025

As proposed by Hu et al. (2014), additional control tests without mimics are carried out to estimate the wave height reduction due to the friction of the flume bed and sidewalls. The first set of control tests is performed without mimics and is further denoted with Y_i . To estimate the possible influence of the relatively high (1.5 cm) stiff bases of the mimics, another series of control tests is executed with the stiff bases of the mimics still in the board, denoted with Z_i .

Influencing parameters

To assess the capacity of the meadow to reduce wave energy, the wave height reduction over the meadow is analysed in combination with the drag forces and the horizontal deflection of the mimics. The impacts of four parameters are evaluated by a sensitivity analysis: (1) the incident wave height, (2) the submergence ratio, (3) the flexural rigidity of the mimics and (4) the wave period.

Five wave heights and five wave periods are applied for the three mimics with different flexural rigidities. The submergence ratio is defined as the ratio of the vegetation height h_s to the water depth h . The latter is taken at the position of the vegetation, as the water depth is reduced due to the elevation of the board, and equals for all tests 0.22 m. Three vegetation lengths (20, 16 and 13 cm) are used for the first and the second mimic, yielding three submergence ratios: 0.91, 0.73 and 0.59. Only the smaller two lengths are applied for the second mimic, which correspond to the lower submergence ratios 0.73 and 0.59. The relatively high submergence ratios are chosen to reduce the relative importance of the stiff mimic base.

Data collection

Wave gauges

Wave gauges are installed along the flume to measure the free surface elevation. The first wave gauge is placed 2 m after the wave paddle to compare the inserted wave height to the actual wave height. The second one stands right after the first one, with a distance between them of 21 cm. The distance may have to change if a different wave period is applied but this was not necessary for the experiments. These wave gauges are installed to compare the measured wave height with the one inserted.

To measure the wave height attenuation of the meadow, wave gauges in the beginning and at the end of the vegetation patch are needed. Due to the limited water height above the vegetation for the relatively high submergence ratios, it is not possible to place the wave gauges at the edges of the meadow without hindering the movement of the leaves. One wave gauge (WG3) is positioned right in front of the vegetation meadow (17 cm) and another one (WG4) right after it (17 cm), as is suggested by Koch et al. (2006). This way, the impact of the vegetation field on the wave height can be determined. The last wave gauge (WG5) is placed another 26 cm after WG4 and is used as substitute of WG4 in case the latter turns out to be affected by edge effects of the meadow.

Force transducers

Three of the mimics are mounted on three sensors that measure the horizontal force at the base in both the positive and negative direction parallel to the direction of the oscillating flow. One transducer is positioned on the first row of mimics perpendicular to the wave propagation direction, another one is placed 30 cm behind the first one and the last transducer is positioned 30 cm behind the second one. All of the force transducers are positioned in the middle of the wave flume, measured in the direction perpendicular to the wave propagation. The positioning of the force transducers can be seen on Figure 13.

These force transducers are hidden in a false bottom to prohibit disturbance of the flow. They consist of a stiff solid platform, carried by two steel cantilever beams, with four temperature-corrected strain gauges mounted in pairs on opposite sides of each of the two steel cantilevers (Bouma et al., 2005). On top of each transducer, a small metal strip is mounted to which the blade is attached with tape, in a way that allows for the natural bending behaviour of the blade. The transducers measure the net instantaneous horizontal force, which is the sum of the drag, the acceleration reaction force and the inertial force. The latter is experienced by flexible organisms moving with the flow when jerked to a halt before changing direction of swing. The force transducers are calibrated by hanging weights of known masses from a string attached to the transducer in both the positive and negative direction, in analogy to Stewart (2004).

Digital camera

A digital camera is set up next to the wave flume to determine the horizontal deflection of the blades in the direction of the oscillating flow. Therefore, a transparent grid of 1 by 1 cm is attached to the sidewall of the wave flume.

Data processing

Wave gauges

The data from the wave gauges is analysed with the software package 'WaveLab (3)', a program that includes time and frequency domain analysis of elevations (Aalborg University, 2017).

The wave height reduction per unit length of meadow is defined as:

$$\Delta H = (H_i - H_j)/x$$

with H_i and H_j the wave height at the wave gauge in front and behind the vegetation respectively and x the distance in between the wave gauges (Paul et al., 2012). With the configuration of the wave gauges as described earlier, the distance between WG3 and WG4 is 1.04 m and the distance between WG3 and WG5 amounts 1.30 m. The dissipation over the vegetation is assumed linear, which is a valid simplification according to Fonseca et al. (1992) for flexible vegetation with relatively small wave-attenuating ability over short distances. To exclude the possible influence of bed and sidewall friction, the wave height reduction corresponding to the control test without vegetation is subtracted from the one with vegetation (Hu et al., 2014).

To estimate the influence of the relatively high stiff bases, the wave height reduction ΔH between WG3 and WG4 of the control tests with (Z) and without the cylinders (Y) are compared. In Figure 14 the wave height reduction is shown in function of the induced wave height, for different values of wave period. As the reduction with the cylinders is for some cases increased and for other cases decreased, no conclusion can be drawn about the influence of the mimic bases. However, for both control test series the wave height between WG3 and WG4 is not reduced but increased for $T = 1.1s$ and $T = 1.7 s$. This is most probably due to reflection at the end of the wave flume and WG4 possibly being positioned at a node of the wave.

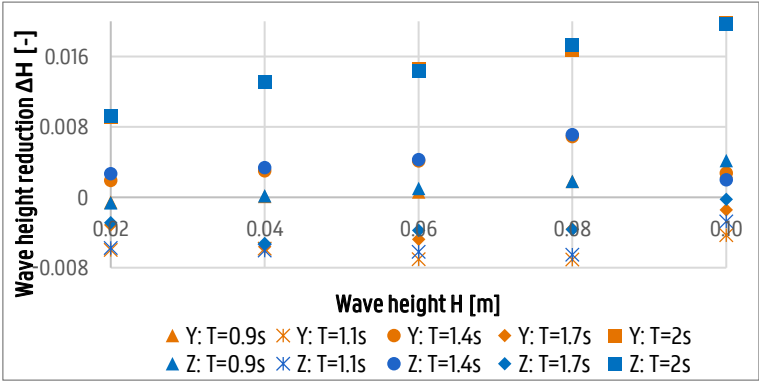


Figure 14: Wave height reduction ΔH between WG3 and WG4 for control tests with (Z) and without stiff mimic bases (Y)

The comparison in wave height reduction between WG3 and WG5 for both control test series is presented in Figure 15. Except for a few cases, the wave height reduction is positive. The overall difference between the Y- and Z-series is smaller compared to the previous graph, apart from the set with wave period 1.4 s. For the further results, the wave height reduction in between WG3 and WG5 will be used and the value of ΔH obtained for the different mimics is reduced by the value of the case without the cylinders (Y) to acquire the effect of the mimics without the effects of flume bed and sidewall friction.

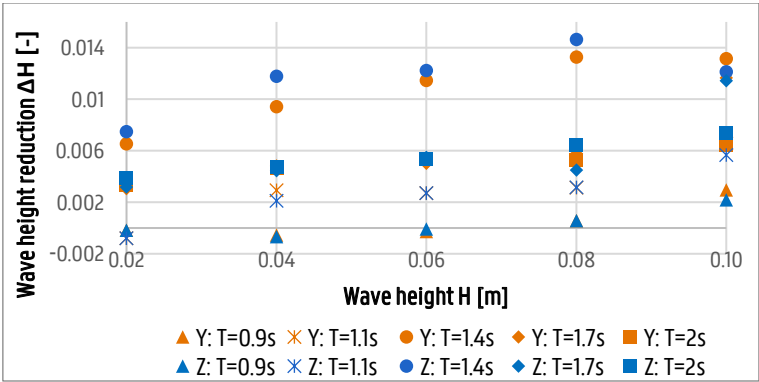


Figure 15: Wave height reduction ΔH between WG3 and WG5 for control tests with (Z) and without stiff mimic bases (Y)

Force transducers

The signals of the drag forces measured by the force transducers are processed with the software 'Matlab R2016a' (The MathWorks, inc., 2016). The original signal of the drag force at the third position for the case F01 is shown on the top right of Figure 16 as an example. A low pass Butterworth filter is designed to reduce the noise on the signal, which has a sample frequency of 40 Hz. Therefore, the frequency domain of the signal is analysed with a discrete Fourier transform (DFT), as can be seen on the left of Figure 16. To retain only the first mode of the signal, a cut-off frequency of 1.5 Hz is chosen for

the filter. The impact on the frequency content of the signal is visible on the middle right of Figure 16. On the bottom of Figure 16, the smoothing effect of the filter with an order of 5 is shown.

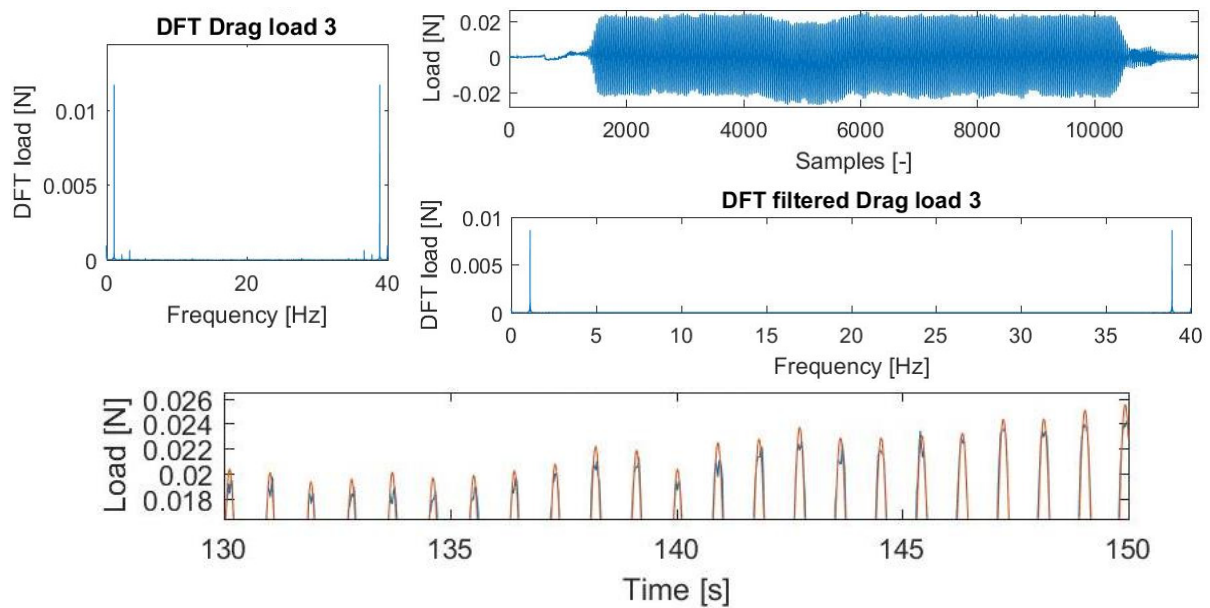


Figure 16: Filter on signal of drag force for case F01

The local extrema of the load signal are collected in an interval for which the signal is relatively stable and the amplitude of the signal is obtained by subtracting the average of the minima from the average of the maxima and dividing this by 2. This is done for all test cases and on all three positions (F1, F2 and F3 as indicated on Figure 13).

Shortening the mimics in between the test series to obtain different submergence ratios decreases the frontal surface area of the mimics and hence reduces the drag on the mimics. To disentangle the influence of shortening the mimics and the influence of the submergence ratio, the drag force is expressed per frontal surface area of the mimic, which is equal to the width of the blades multiplied by the length (stem base height not included).

Digital camera

Each test is recorded with the digital camera positioned in a way that transparent grid is clearly visible and parallel with the line of mimics in the middle of the meadow. The bending is defined by the angle from the horizontal, meaning that stiff, non-bending leaves are approximately 90° to the horizontal, whereas flexible, fully bent leaves approach 0°. The angle is calculated as the arctangent of dy/dx , with dy the vertical distance and dx the horizontal distance between blade tip and the place of attachment to the base. This way, the shape of the curve for bent leaves is approximated by a straight line (Bouma et al., 2005). Figure 17 illustrates how the bending angle is defined.

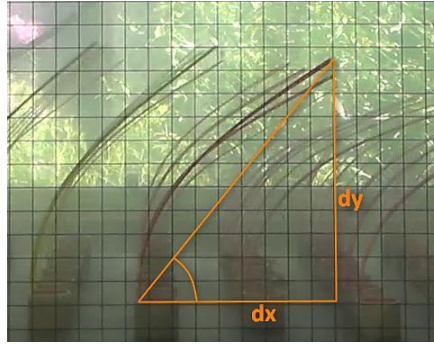


Figure 17: Definition of bending angle

For each test case, the distances are determined from the video-recordings by averaging 10 extreme values in a range for which the waves are fully developed. Care is taken that this range corresponds to the range used for the selection of extrema from the load signals. The horizontal displacements are found by measuring the distance in between positive and negative tip displacements and dividing the obtained value by two. This assumes a symmetrical movement of the blade relative to its original position.

Chapter 5: Sensitivity analysis

Drag force

As explained before, the drag force is measured at three positions (F_1 , F_2 and F_3 with the locations indicated on Figure 13) and is divided by the frontal surface area of the blade. The values of the drag force per frontal surface area at the first position in function of the wave height are presented in Figure 19, split up for different wave periods and different mimics. The R^2 -value of the linear regressions for each submergence ratio are indicated and for all graphs the same legend is used, shown in the top left corner. The graphs on Figure 19 are used to estimate the influence of incident wave height, submergence ratio and flexural rigidity on the drag force in the following paragraphs.

Influence of force transducer position

To analyse the differences between the positions, the drag forces per frontal surface area are plotted in function of the wave height in Figure 18 for the different mimics. The graph correspond to the test cases with wave period equal to 0.9 s but the same behaviour is observed for all wave periods.

For all mimics the drag force is highest at the beginning of the meadow, which corresponds to the expectations as the first row of mimics is not sheltered by anything in front.

For mimics 2 and 3 the drag decreases towards position 2 and subsequently towards position 3, i.e. $F_1 > F_2 > F_3$. Hence the drag force reduces over the entire length of the meadow. The reduction of the drag force increases with increasing wave height, which is concluded from the varying slopes for the different positions.

Mimic 1, however, encounters the lowest drag force in the middle of the meadow instead of at the end, i.e. $F_1 > F_3 > F_2$, although the differences are rather small. This could be explained by a slight difference in flexural rigidity between the mimics obtained from different notebooks, with the mimic on force transducer 2 having a slightly smaller flexural rigidity. To study the influence of different parameters on the drag force, the effect of a slightly different flexural rigidity is excluded by examining the drag force at the first position.

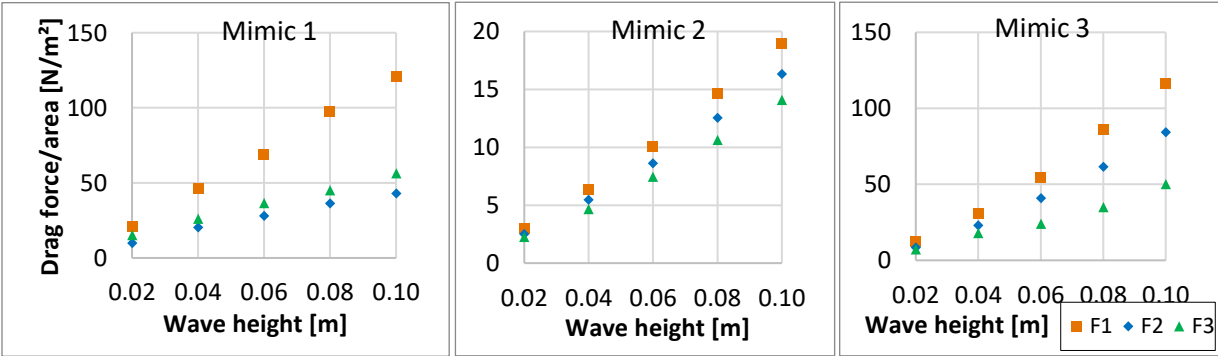


Figure 18: Analysing the influence of the force transducer position

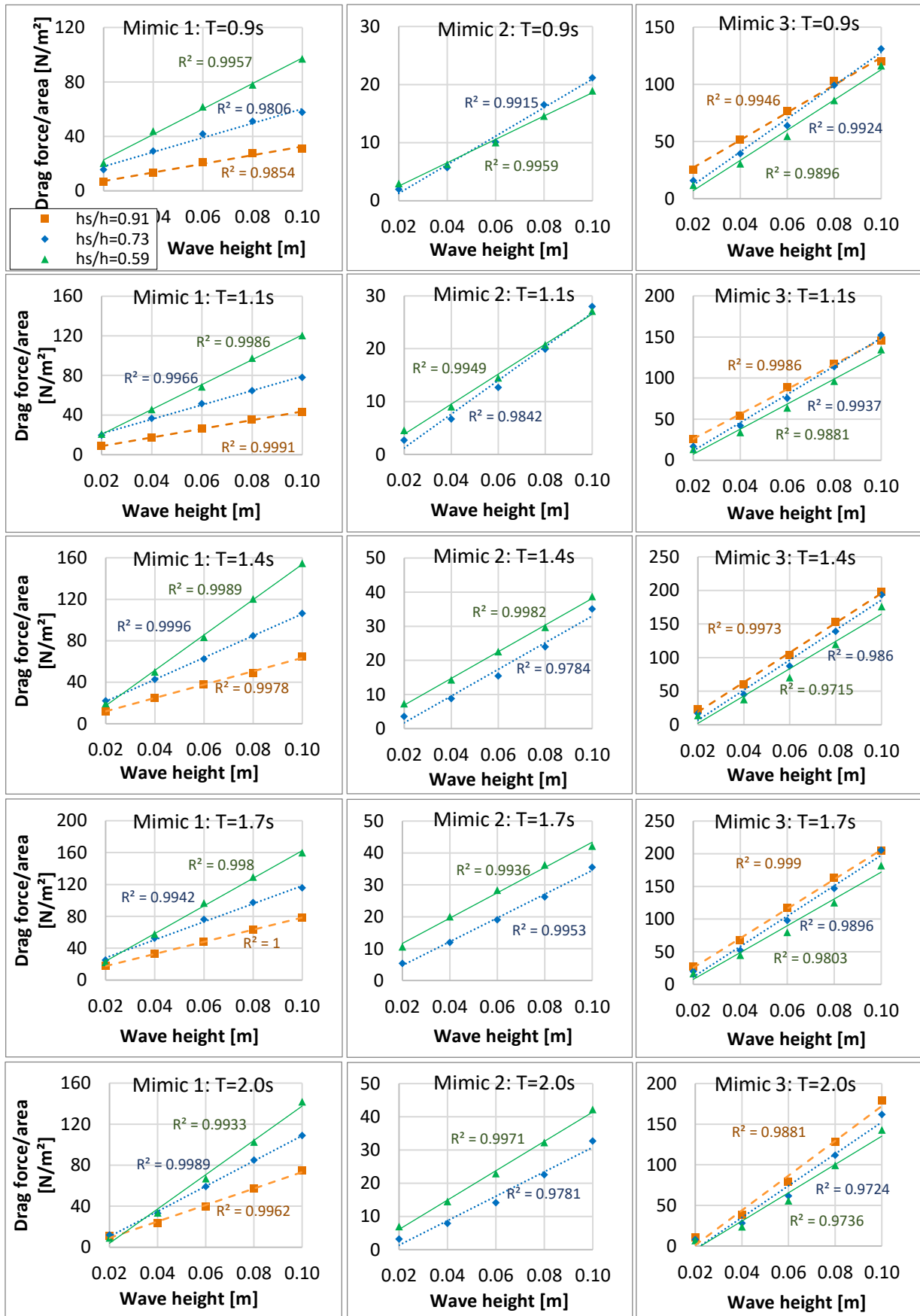


Figure 19: Drag force per frontal surface area at position 1 in function of wave height for different mimics and wave periods

Influence of wave height

As expected, the drag forces on all three positions increase with increasing wave height, for all test cases. The linear regression lines show an exceptional correlation, with R^2 -values approaching unity. The largest value of the drag force per frontal surface area is found for cases F24 and G24 and equals 205 N/m^2 .

Influence of submergence ratio

For low submergence ratios, the leaves are lower in the water column where they are exposed to less orbital motion. Therefore, it is expected that the drag force decreases with decreasing submergence ratio. This relationship is indeed observed for the third mimic, for which the highest drag force is obtained for the highest submergence ratio. Two cases with a relatively high wave height and low wave period (i.e. a high wave steepness) make the exception, which is probably due to the reflection at the end of the wave flume for these wave conditions. The differences remain rather constant with the wave height, i.e. the slopes of the regression lines are comparable, although the difference between the two lower submergence ratios increases with increasing wave height.

However, the opposite holds for the other two (more flexible) mimics, for which the drag force decreases with increasing submergence ratio, except for 4 cases with the highest waves and low wave periods. For mimic 2 the differences between the drag force for the different submergence ratios remain almost constant, whereas the differences increase with increasing wave height for mimic 1. Analysing the video-recordings of mimics 1 and 2 for varying submergence ratios reveals that the flexible leaves are pushed over by the wave-induced flow. The more streamlined shape in combination with the reduced frontal area results in a reduced drag. This phenomenon is also called reconfiguration (Luhar and Nepf, 2011) and becomes more pronounced for longer leaf lengths. The phenomenon of reconfiguration can be seen on Figure 25 where it is discussed more thoroughly. Due to this increased reconfiguration with increasing submergence ratio, the drag force decreases with increasing submergence ratio for the two more flexible mimics.

Influence of flexural rigidity

A clear distinction can be made between the different mimics with varying flexural rigidity. The left graph on Figure 20 shows the relationship with more detail. Mimic 3, with the highest flexural rigidity, encounters the highest drag forces and this difference increases with wave height. Mimic 1 experiences the second-highest forces followed by mimic 2, which is the most flexible one. One can conclude that the drag force increases with increasing flexural rigidity and the differences enlarge with increasing wave height. This corresponds with the results of Bouma et al. (2005).

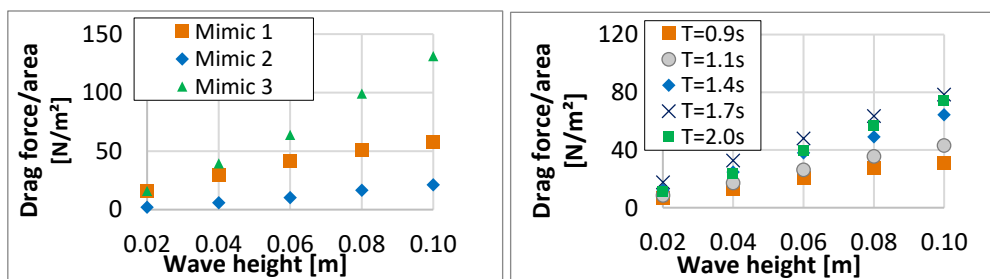


Figure 20: Analysing the influence of (left) flexural rigidity on (right) wave period on the drag force

Influence of wave period

From Figure 20 it is obtained that the drag force increases with increasing wave period until the wave period equals 1.7 s, after which it decreases again for a wave period of 2.0 s. This conclusion is true for all mimics and all submergence ratios.

Wave height reduction

As mentioned earlier, the wave height reduction is determined between WG3 and WG5. The wave height reduction in function of the wave height is given in Figure 21 for all different wave periods and submergence ratios. The R^2 -value of the linear regressions for each test case are indicated and the same legend is used for all graphs, displayed on the upper left graph. Figure 21 will be used in the next paragraphs to analyse the influence of incident wave height, submergence ratio, flexural rigidity and wave period on the wave height attenuation.

Influence of wave height

The largest obtained wave height reduction equals 0.99% and is found for test case F08. A general trend is observed for which the wave height reduction increases with increasing wave height. This relationship is particularly clear for mimic 1, which yields the highest correlation and shows the relationship for all submergence ratios.

However, the increase of ΔH with increasing H does not hold for all cases and the linear regression lines are only given for the cases with an acceptable R^2 -value (i.e. ≥ 0.65). For the tests with wave period above 1.4 s and/or wave height above (0.06-)0.08 m, the results are not clear. For a number of test conditions, the wave height reduction drastically decreases when the wave height equals 0.10 m and even becomes negative for two of them. This result is observed over all submergence ratios and concerns all mimics. The larger wave period yields shallower wave conditions, with relative water depth at the position of the vegetation $h/\lambda \leq 0.09$. Possible effects induced by the shallower wave conditions may explain the different results for higher wave periods. Another explanation could be the increased wave reflection and the end of the wave flume for these wave conditions. Omitting the values of those particular tests would increase the correlation for the relationship between the wave height reduction and the incident wave height.

Influence of submergence ratio

For high submergence ratios, the vegetation takes up more of the water column, hence it is expected that the wave height attenuation increases with increasing submergence ratio. For most cases of mimics 2 and 3, the attenuation is indeed found to be increasing with increasing submergence ratio, except for the cases with contradicting values discussed in the previous paragraph. However, this relationship is not observed for mimic 1, for which in some cases the opposite holds. This matches with what was found for the influence of the submergence ratio on the drag force.

Influence of flexural rigidity

The mimic with the highest flexural rigidity is expected to be most capable of attenuation waves. Mimic 3 yields indeed the largest wave height attenuation for the two highest submergence ratios (and $T \leq 1.4$ s), with the differences increasing with increasing wave height. Nonetheless, for a wave period equal to 2.0s, the highest reduction is found by mimic 1, for all submergence ratios. However, as discussed earlier, the test cases with wave period above 1.4 s yield disconcerting results, especially for wave heights starting from 0.08 m.

For other test conditions, no clear distinction between the mimics can be found. Although mimic 2 offers for none of the cases the largest wave height reduction, it does not always provide the lowest attenuation. For completeness, a comparison between the different mimics can be found in Figure 27 in the Appendix.

Influence of wave period

As discussed earlier, the test cases with wave period above 1.4 s yield disconcerting results, especially for wave heights starting from 0.08 m. No clear connection between the wave period and the wave height decay is obtained, although the wave height reduction for the cases with wave period equal to 2.0 s is generally lower compared to other cases. This corresponds with the reduction of drag forces found for the same cases.

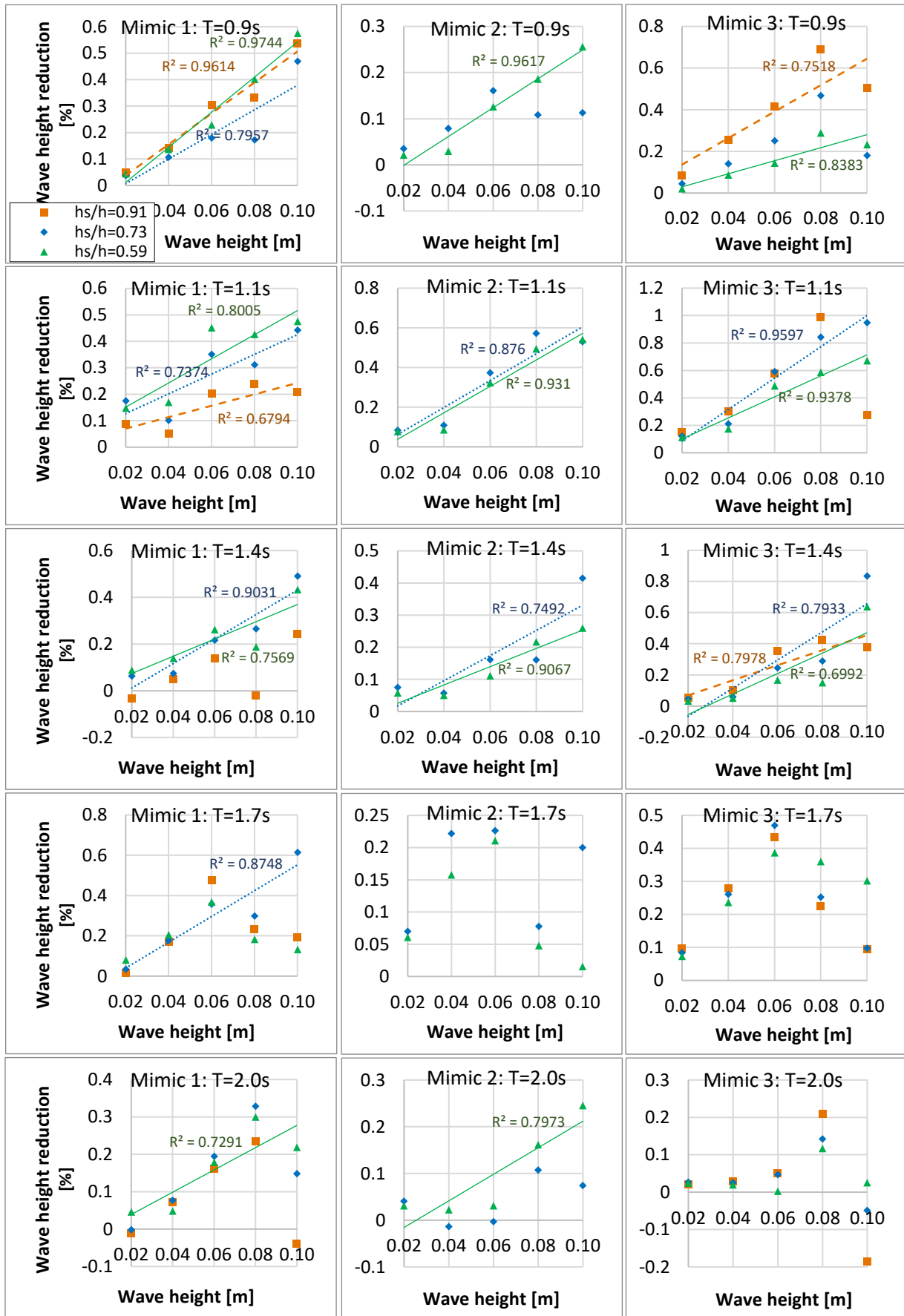


Figure 21: Wave height reduction in function of wave height for different wave periods and mimics

Bending angle

Figure 22 presents the bending angle (i.e. the angle with the horizontal) in function of the wave height for all different wave heights and submergence ratios. The same legend is used for all graphs, shown in the upper left corner. This figure will be used in the next paragraphs to analyse the influence of the wave height, submergence ratio, flexural rigidity and wave period on the bending angle.

Influence of wave height

It is expected that the bending angle decreases with increasing wave height. This is confirmed and a highly correlated relationship is observed, with R^2 -values close to unity for most cases.

The correlation is lower for series D, i.e. the most flexible mimic with a submergence ratio of 0.73. For this series the values obtained under incident wave heights of 0.08 and 0.10 m are somewhat higher than expected. Re-analysing the video-recordings for series D reveals that the mimics remain bended in the direction of wave propagation, without being able to bend in the other direction or even to return to the original position for all tests with mimic 2. Due to this asymmetric behaviour, the horizontal displacement is reduced, which results in the observed higher bending angle. This feature reveals that the flexural rigidity of the blades is not a parameter on its own, but needs to be considered in combination with the induced blade motion. Paul et al. (2012) already stated that the type of motion (cantilever versus whip-like) might be more important for wave attenuation than the material stiffness as such.

Influence of submergence ratio

For high submergence ratios, the leaves are higher in the water column where they are exposed to more orbital motion. Therefore, it is expected that the bending angle, i.e. the angle with the horizontal, decreases with increasing submergence ratio. For mimic 3 and most cases of mimic 1, the bending angle decreases as expected with increasing submergence ratio and the differences enlarge with incident wave height.

The opposite relationship is observed for mimic 2. However, as explained earlier, the leaves remain bended in the direction of wave propagation for series D, which results in a larger bending angle. Due to this phenomenon, the bending angle increases for the higher submergence ratio. Tests with more submergence ratios are required to investigate the relationship between this residual bending and the submergence ratio.

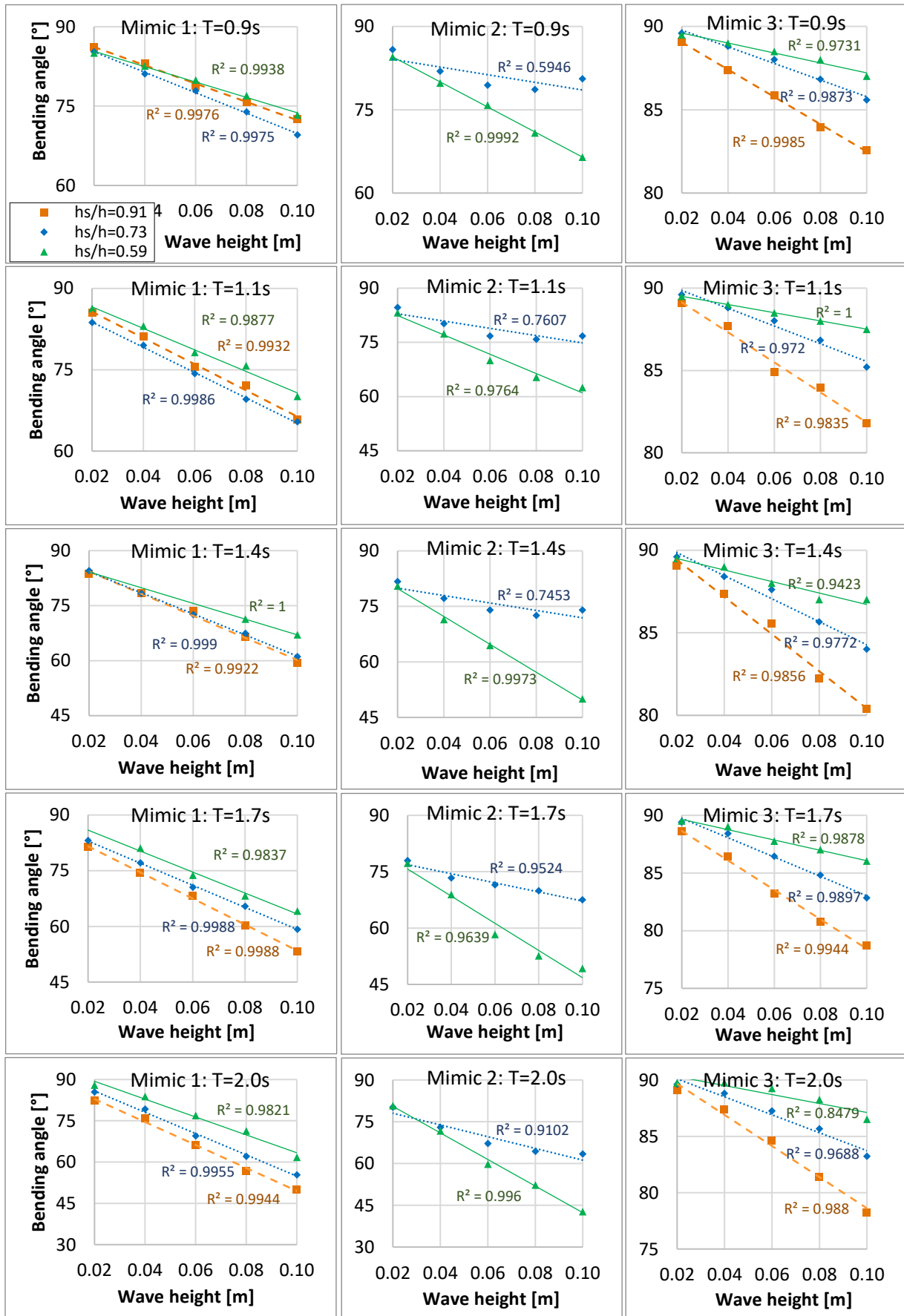


Figure 22: Bending angle in function of wave height for different wave periods and mimics

Influence of flexural rigidity

It can be observed on Figure 22 that the bending angle varies with the flexural rigidity of the blades. To analyse this relationship more thoroughly, the bending angle is given in function of the wave height in Figure 23, comparing the different mimics over the different submergence ratios. The graphs are given for a wave period of 0.9 s, but the same behaviour is observed for all wave periods. The complete overview can be found on Figure 28 in appendix .

The bending angle increases with increasing flexural rigidity for submergence ratios 0.91 and 0.59. However, the bending angle of the second mimic is higher compared to the first mimic for a submergence ratio equal to 0.73. This is again explained by the residual bending of the blades for series D, which results in a higher bending angle.

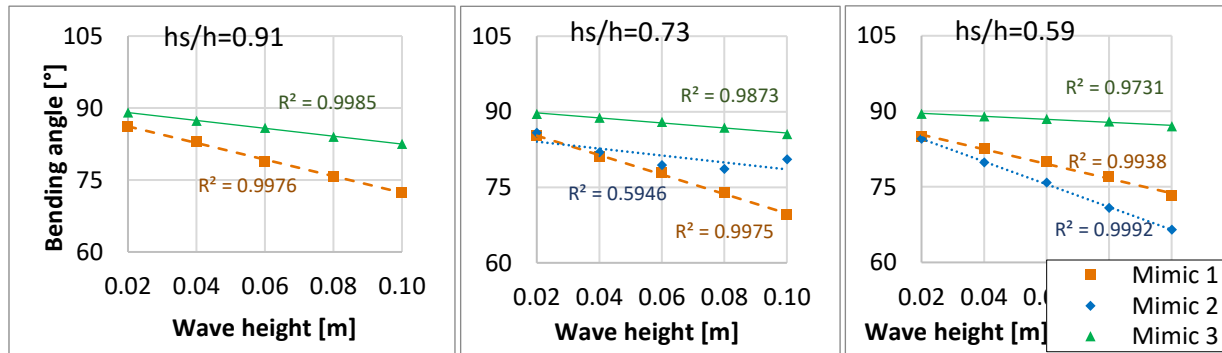


Figure 23: Analysing the influence of the flexural rigidity on the bending angle

Influence of wave period

From Figure 22 can be concluded that the bending angle decreases with increasing wave period, for all test cases. To investigate this relationship in detail, Figure 24 shows the bending angle in function of the wave height for series A, i.e. mimic 1 with a submergence ratio of 0.91, although the same conclusions can be drawn for the other series. The bending angle decreases with increasing wave period, and the differences enlarge with increasing wave height.

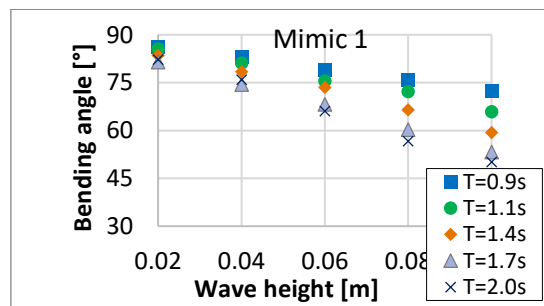


Figure 24: Analysing the influence of the wave period on the bending angle

Combining the drag force, wave height reduction and bending angle

The previous paragraphs analysed the influence of the wave height, submergence ratio, flexural rigidity and wave period on the drag force, the wave height reduction and the bending angle separately. However, these measurements concern the same physical experiments and relationships between them are of major importance.

Figure 25 shows the drag force per frontal surface area in function of the bending angle for the different test series from Table 8. The values are obtained by averaging the data over every series. Series D, indicated in red, yields inconclusive values due to the residual bending. As explained earlier, the leaves remain pronated in the direction of wave propagation for this test series, which results in a reduced horizontal displacement and hence a higher bending angle. Excluding this series, a relationship is detected between the drag force and the bending angle ($R^2 = 0.73$): the higher the bending angle,

the higher the drag force. Both the drag force and the bending angle increase with increasing flexural rigidity; as the flexibility increases, the leaves tend to avoid the drag by bending over (also called reconfiguration), which yields a lower bending angle and lower drag force. This confirms what was found by Bouma et al. (2005) and Paul et al. (2012).

The reconfiguration is enhanced for higher submergence ratios, hence both the drag force and the bending angle decrease with increasing submergence ratio for the flexible mimics. This movement is not observed for the stiffer mimic 3, for which the drag force increases with increasing submergence ratio, while the bending angle decreases. No conclusion about the bending angle could be drawn for the second mimic due to the residual bending in series D.

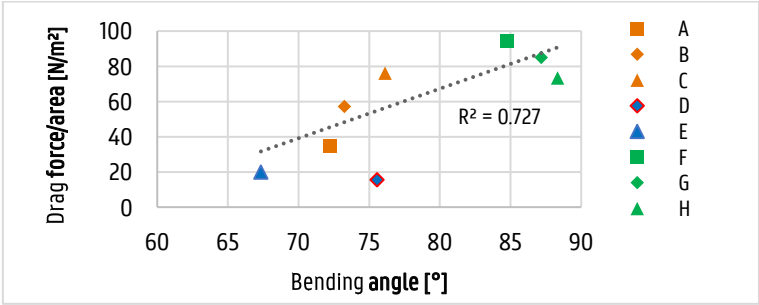


Figure 25: Drag force per frontal surface area in function of bending angle for different test series

Figure 26 shows the relationship between the wave height reduction and the drag force per frontal surface area for the different test series, with a very good correlation ($R^2 = 0.92$).

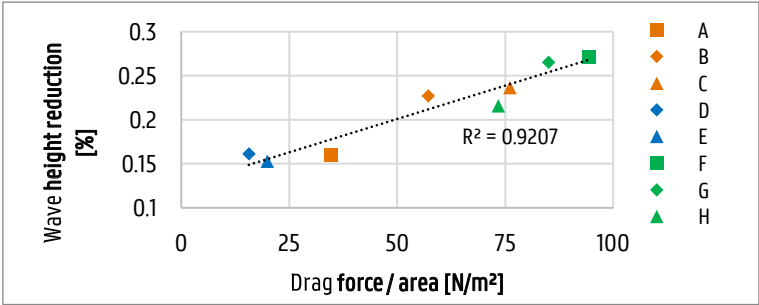


Figure 26: Wave height reduction in function of drag force per frontal surface area for different test series

Conclusion

The wave-attenuating ability of the meadow depends on the wave conditions to which it is subjected. Under larger wave heights and/or wave periods (within a restricted range), the drag force increases and hence an enhanced wave attenuation is obtained.

The wave attenuation can also be assessed from the design characteristics of the meadow. From the previous, the drag force decreases by either decreasing the submergence ratio of the stiffer mimic, by reducing the flexural rigidity of the leaves or by increasing the submergence ratio of the flexible mimic and in such a way enhancing the reconfiguration of the blades. The lower the drag force per frontal surface area, the lower the capacity of the meadow the attenuate waves.

References

- Aalborg University, Hydraulic & Coastal Engineering Laboratory, 2017. WaveLab (3) [Software]
- Anderson, M.E., Smith, J.M., McKay, S.K., 2011. Wave dissipation by vegetation. *US Army Corps of Engineers*. 1-82
- Anderson, M.E., Smith, J.M., 2014. Wave attenuation by flexible, idealized salt marsh vegetation. *Coastal Engineering* 83, 82-92.
- Arnaud-Haond, S., Duarte, C.M., Diaz-Almela, E., Marba, N., Sintes, T., et al., 2012. Implications of Extreme Life Span in Clonal Organisms: Millenary Clones in Meadows of the Threatened Seagrass *Posidonia oceanica*. *PLoS ONE* 7(2): e30454
- Asano, T., Deguchi, H., Kobayashi, N., 1992. Interaction between water waves and vegetation. *Coastal Engineering Conference*. 3, 2710-2710, American Society of Civil Engineers, New York.
- Asano T., S. Tsutsui and T. Sakai, 1988. Wave damping characteristics due to seaweed, *Proc. 35th Coast. Engineering Conference in Japan*, 138-142.
- Augustin, L.N., J.L. Irish, and P. Lynett, 2009. Laboratory and numerical studies of wave dampening by emergent and near-emergent wetland vegetation. *Coastal Engineering* 56, 332-340.
- Bashford, D.P., 1996. *Thermoplastics: directory and databook*. London, UK: Chapman and Hall
- Borum, J., Duarte, C.M., Krause-Jensen, D., Greve, T.M., 2004. *European Seagrasses: an Introduction to Monitoring and Management*. A publication by the EU project Monitoring and Managing of European Seagrasses (M&MS).
- Bouma, T., Temmerman, S., van Duren, L., Martini, E., Vandenbruwaene, W., Callaghan, D., Balke, T., Biermans, G., Klaassen, P., van Steeg, P., et al., 2013. Organism traits determine the strength of scale-dependent bio-geomorphic feedbacks: a flume study on three intertidal plant species. *Geomorphology* 180, 57-65.
- Bouma, T.J., De Vries, M.B., Low, E., Peralta, G., Tanczos, C., Van de Koppel, J., Herman, P.M.J., 2005. Trade-offs related to ecosystem engineering: a case study on stiffness of emerging macrophytes. *Ecology* 86, 2187-2199.
- Bradley, K., Houser, C., 2009. Relative velocity of seagrass blades: Implications for wave attenuation in low-energy environments, *Journal of Geophysical Research* 01004, 114
- Buia, M.C., Gambi, M.C., Dappiano, M., 2004. Seagrass Systems, in: Gambi, M.C., Dappiano, M. (Eds.), *Mediterranean Marine Benthos: A Manual of Methods for its Sampling and Study*. Societa' Italiana di Biologia Marina, Genova, 604.
- Chen, S.H., Sanford, L.P., Koch, E.W., Shi, F., North, E.W., 2007. A nearshore model to investigate the effects of seagrass bed geometry on wave attenuation and suspended sediment transport. *Estuaries and Coasts* 30, 296-310.
- Dalrymple, R.A., Kirby, J.T., Hwang, P.A., 1984. Wave diffraction due to areas of energy-dissipation. *Journal of Waterway Port Coastal and Ocean Engineering* 110, 67-79.
- Dijkstra, J.T., Uittenbogaard, R.E., 2010. Modeling the interaction between flow and highly flexible aquatic vegetation. *Water resources research* 46, W12547
- Dubi, A., Torum, A., 1997. Wave energy dissipation in kelp vegetation, *Proceedings of the Twenty-Fifth Coastal Engineering Conference* B. L. Edge, 2626-2639 American Society of Civil Engineering, New York.
- Elginos, N., Kabdasli, M.S., Tanik, A., 2011. Effects of *Posidonia oceanica* seagrass meadows on storm waves. *Journal of Coastal Research* SI 64, 373-377.
- Folkard, A.M., 2005. Hydrodynamics of model *Posidonia oceanica* patches in shallow water. *Limnology and Oceanography* 50, 1592-1600.
- Fonseca M.S., Cahalan J.A., 1992. A preliminary evaluation of wave attenuation by four species of seagrasses. *Estuarine, Coastal and Shelf Science* 35, 565-576.
- Ghisalberti, M., Nepf, H.M., 2002. Mixing layers and coherent structures in vegetated aquatic flows. *Journal of Geophysical Research: Oceans* 107 (C2), 1-11.
- Green, E.P., Short, F.T., 2003. *World Atlas of Seagrasses*. Prepared by the UNEP World Conservation Monitoring Centre. University of California Press, Berkeley, USA.
- Houser, C., Trimble, S. & Morales, B., 2015. Influence of Blade Flexibility on the Drag Coefficient of Aquatic Vegetation. *Estuaries and Coasts* 38, 569-577.
- Hu, Z., Suzuki, T., Zitman, T., Uittewaal, W., Stive, M., 2014. Laboratory study on wave dissipation by vegetation in combined current-wave flow. *Coastal Engineering* 88, 131-142.
- Infantes, E., Orfila, A., Simarro, G., Terrados, J., Luhar, M., & Nepf, H.M., 2012. Effect of a seagrass (*Posidonia oceanica*) meadow on wave propagation. *Marine Ecology Progress Series* 456, 63-72.
- John, B.M., Shiralal, K.G., Rao, S., Rajasekaran, C., 2016. Effect of artificial seagrass on wave attenuation and wave run-up. *The International Journal of Ocean and Climate Systems* 7, 14-19.

- Knutson, P.L., Brochu, R.A., Seelig, W.N., Inskip, M., 1982. Wave damping in *Spartina alterniflora* marshes. *Wetlands* 2, 87-104.
- Kobayashi, N., A.W. Raichle, and T. Asano., 1993. Wave attenuation by vegetation. *Journal of Waterway, Port, Coastal, and Ocean Engineering* 119, 30–48.
- Koch, E.W., Sanford, L.P., Chen, S.N., Shafer, D.J., Smith, J.M., 2006. Waves in seagrass systems: review and technical recommendations. US Army Corps of Engineers, 1-92.
- Koch, E.W., Barbier, E.B., Silliman, B.R., Reed, D.J., Perillo, G.M., Hacker, S.D., Granek, E.F., Primavera, J.H., Muthiga, N., Polasky, S., Halpern, B.S., Kennedy, C.J., Kappel, C.V., Wolanski, E., 2009. Non-linearity in ecosystem services: temporal and spatial variability in coastal protection. *Frontiers in Ecology and the Environment* 7, 29-37.
- Koftis, T., Prinos, P., Stratigaki, V., 2013. Wave damping over artificial *Posidonia oceanica* meadow: A large-scale experimental study. *Coastal Engineering* 73, 71-83.
- Li, C.W., Yan, K., 2007. Numerical investigation of wave-current-vegetation interaction. *Journal of Hydraulic Engineering* 133, 794–803.
- Luhar, M., Coutu, S., Infantes, E., Fox, S., Nepf, H.M., 2010. Wave-induced velocities inside a model seagrass bed. *Journal of Geophysical Research* 115 (C12005), 1–14.
- Luhar, M., Nepf, H.M., 2011, Flow-induced reconfiguration of buoyant and flexible aquatic vegetation, *Limnology and Oceanography*, 56(6), 2003–2017.
- Luhar, M., Nepf, H.M., 2016, Wave-induced dynamics of flexible blades, *Journal of Fluids and Structures* 61, 20–41.
- Luhar, M., E. Infantes, and H. Nepf, 2017, Seagrass blade motion under waves and its impact on wave decay, *Journal of Geophysical Research: Oceans* 122, 3736–3752.
- Maltese, A., Cox, E., Folkard, A.M., Ciraolo, G., La Loggia, G., Lombardo, G., 2007. Laboratory measurements of flow and turbulence in discontinuous distributions of ligulate seagrass. *Journal of Hydraulic Engineering - ASCE* 133, 750–760.
- Manca, E., 2010. Effects of *Posidonia oceanica* seagrass on nearshore waves and wave-induced flows. University of Southampton, School of Ocean and Earth Science, Doctoral Thesis , 332.
- Mansard, E.P.D., Funke, E.R., 1980. The measurement of incident and reflected spectra using a least squares method. *Coastal Engineering* Mark, J.E., 2009. *Polymer Data Handbook* (2nd edition). Oxford, UK: Oxford University Press, Inc.
- Maza, M., Lara, J.L., Losada, I.J., 2016. Solitary wave attenuation by vegetation patches. *Advances in Water Resources* 98, 159-172
- Mendez, F.J., Losada, I.J., 2004. An empirical model to estimate the propagation of random breaking and non-breaking waves over vegetation fields. *Coastal Engineering* 51, 103–118.
- Mendez, F.J., Losada, I.J., Losada, M.A., 1999. Hydrodynamics induced by wind waves in a vegetation field. *Journal of Geophysical Research* 104(8), 18383–18396.
- Möller, I., Kudella, M., Rupprecht, F., Spencer, T., Paul, M., van Wesenbeeck, B.K., Wolters, G., Jensen, K., Bouma, T.J., Miranda-Lange, M., Schimmels, S., 2014. Wave attenuation over coastal salt marshes under storm surge conditions. *Nature Geoscience* 7(10), 727-731.
- Morison, J. R., Johnson, J. W., Schaaf, S.A., 1950. *The Force Exerted by Surface Waves on Piles*. Society of Petroleum Engineers.
- Mullarney, J. C., Henderson, S.M., 2010. Wave-forced motion of submerged single-stem vegetation, *Journal of Geophysical Research* 12061, 115.
- Ota, T., Kobayashi, N., Kirby, J.T., 2004. Wave and current interactions with vegetation. *Proc. Int. Conf. Coastal Eng. Lisbon*, 508-520. ASCE, New York.
- Paul, M., Bouma, T., & Amos, C., 2012. Wave attenuation by submerged vegetation: Combining the effect of organism traits and tidal current. *Marine Ecology Progress Series* 444, 31-41.
- Paul, M., Rupprecht, F., Möller, I., Bouma, T., Spencer, T., Kudella, M., Wolters, G., van Wesenbeeck, K., Jensen, K., Schimmels, S., 2016. Plant stiffness and biomass as drivers for drag forces under extreme wave loading: A flume study on mimics, *Coastal Engineering* 117, 70-78.
- Riffe, K.C., Henderson, S.M., Mullarney, J.C., 2011. Wave dissipation by flexible vegetation, *Geophysical Research Letters*, 38, L18607
- Rupprecht, F., Möller, I., Evans, B., Spencer, T., Jensen, K., 2015. Biophysical properties of salt marsh canopies — quantifying plant stem flexibility and above ground biomass. *Coastal Engineering* 100, 48–57.
- Sánchez-González, J.F., Sánchez-Rojas, V., Memos, C.D., 2011. Wave attenuation due to *Posidonia oceanica* meadows. *Journal of Hydraulic Research* 49, 503–514.
- Stewart, H.L. (2004) Hydrodynamic consequences of maintaining an upright posture by different magnitudes of stiffness and buoyancy in the tropical alga *Turbinaria ornata*. *Journal of Marine Systems* 49, 157–167.
- Stratigaki, V., Manca, E., Prinos, P., Losada, I.J., Lara, J.L., Sclavo, M., Amos, C.L., Caceres, I., Sanchez-Arcilla, A., 2011. Large-scale experiments on wave propagation over *Posidonia oceanica*. *Journal of Hydraulic Research* 49, 31–43.

- Suzuki, T., Zijlema, M., Burger, B., Meijer, M.C., Narayan, S., 2012. Wave dissipation by vegetation with layer schematization in SWAN. *Coastal Engineering* 59, 64-71.
- The Mathworks, Inc., 2016. MATLAB R2016a (9.0.0.341360) [Software].
- Vacchi, M., De Falco, G., Simeone, S., Montefalcone, M., Morri, C., Ferrari, M., and Bianchi, C.N., 2017. Biogeomorphology of the Mediterranean *Posidonia oceanica* seagrass meadows. *Earth Surface Processes and Landforms* 42, 42-54.
- Zeller, R. B., J. S. Weitzman, M. E. Abbett, F. J. Zarama, O. B. Fringer, and J. R. Koseff. 2014. Improved parameterization of seagrass blade dynamics and wave attenuation based on numerical and laboratory experiments. *Limnology and Oceanography* 59, 251-266.

Appendix A

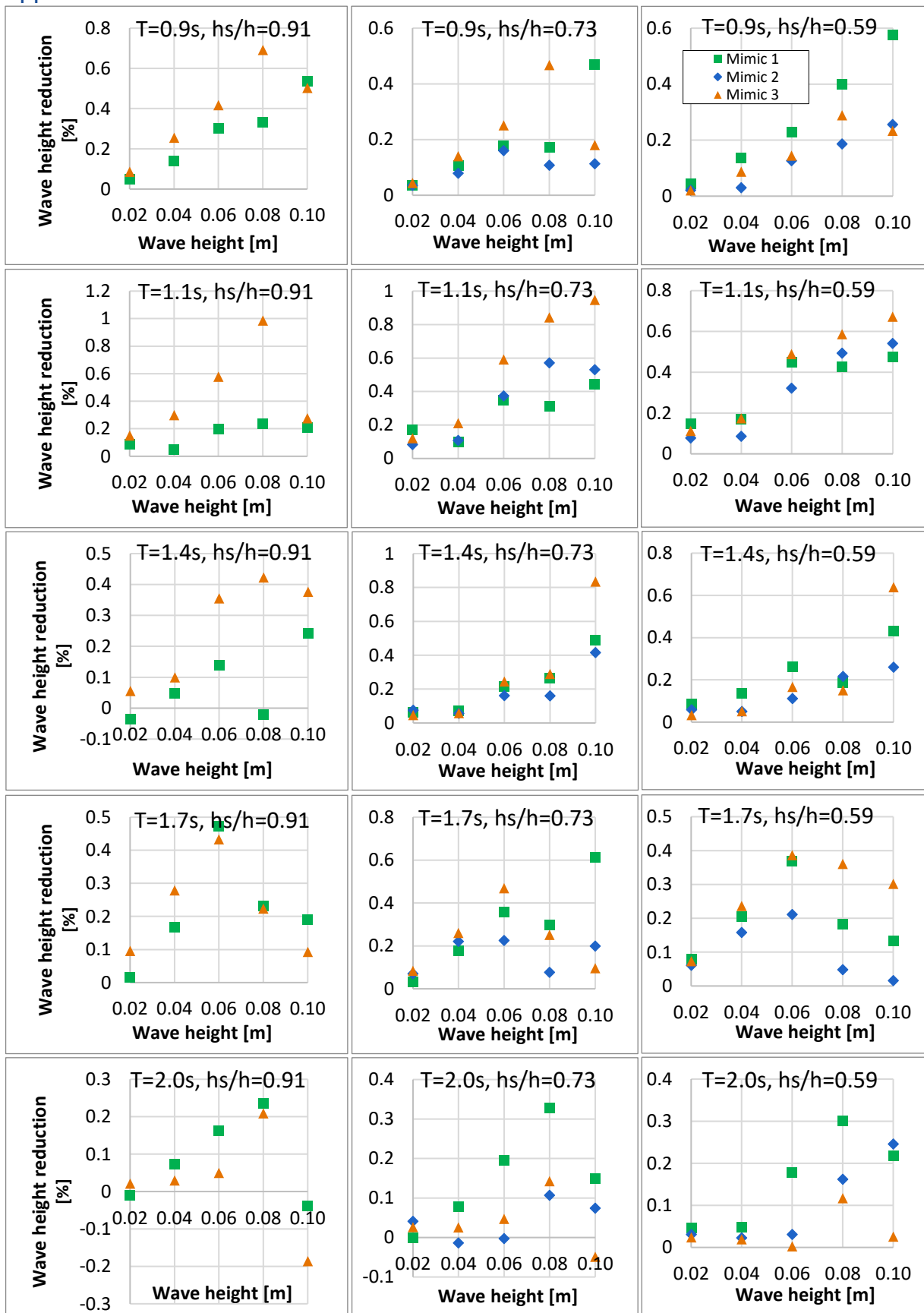


Figure 27: Wave height reduction in function of wave height for different wave periods and different submergence ratios

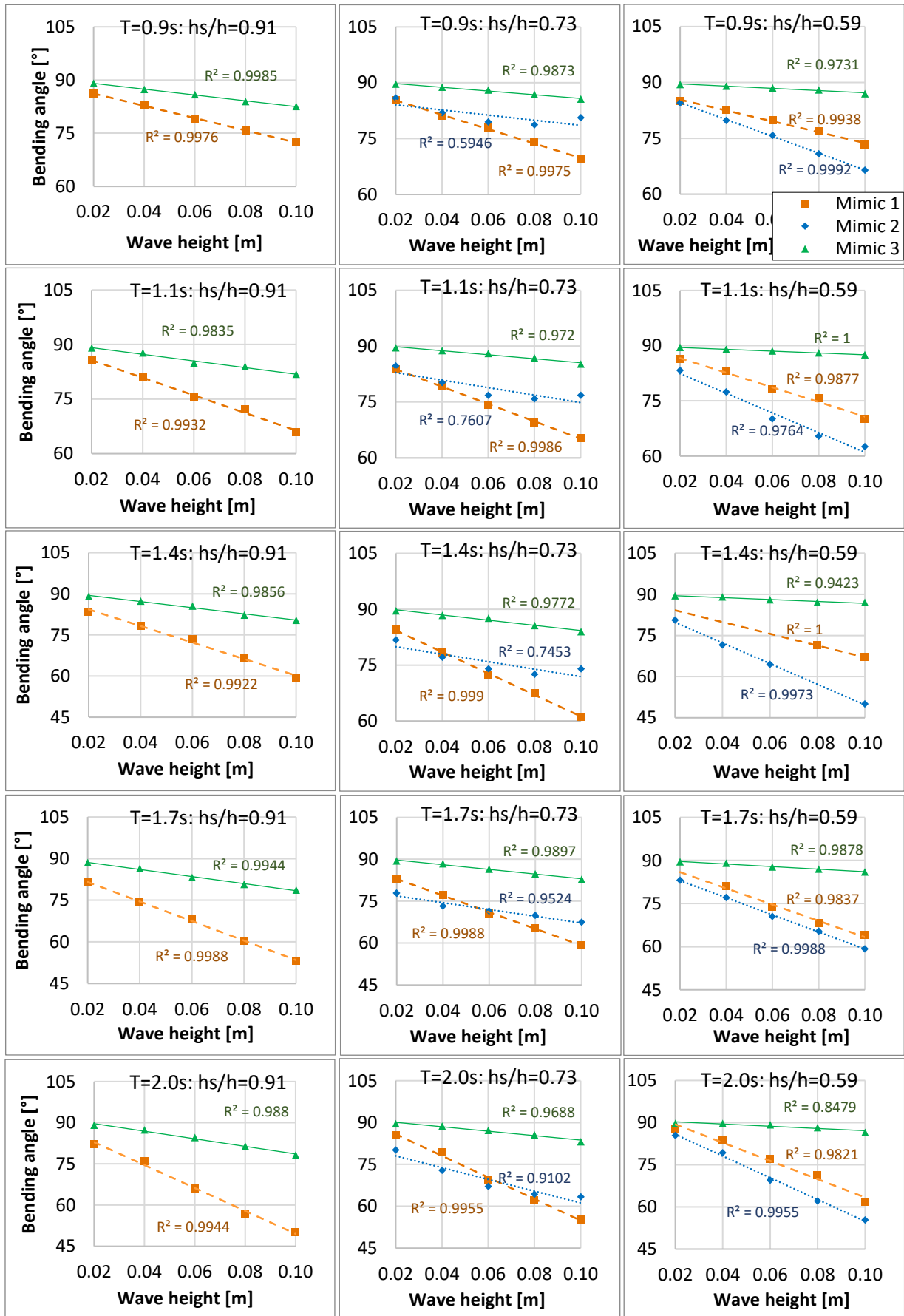


Figure 28: Bending angle in function of wave height for different wave periods and different submergence ratios